Aus der Klinik für Neurochirurgie

Direktor: Prof. Dr. Christopher Nimsky

des Fachbereichs Medizin der Philipps-Universität Marburg

Titel der Dissertation:

Investigation on the optimization approaches of diffusion weighted imaging

Inaugural-Dissertation zur Erlangung des Doktorgrades der gesamten Humanmedizin

dem Fachbereich Medizin der Philipps-Universität Marburg

vorgelegt von

Jia Yang

aus Henan, VR China

Marburg, 2019

Angenommen vom Fachbereich Medizin der Philipps-Universität Marburg

am: 15.10.2019

Gedruckt mit Genehmigung des Fachbereichs Medizin

Dekan: Prof. Dr. Helmut Schäfer

Referent: Prof. Dr. Christopher Nimsky

Korreferent: Prof. Dr. Andreas Jansen

This is dedicated to all the uncertain and uncompromising days.

Contents

ABBREVIATION 1

LIST OF FIGURES 2

LIST OF TABLES 3

1. INTRODUCTION 4

1.1 Background: Diffusion weighted imaging, diffusion tensor imaging, and tractography 4

1.2 Application of the DWI and DTI in neuroscience 6

1.3 Disadvantages of DWI 7

1.4 Objectives of this study 7

1.5 Background and objectives of part 1 8

1.6 Background and objectives of part 2 9

2. MATERIALS AND METHODS 12

2.1 Participants 12

2.2 MRI acquisition 12

2.3 Methods in study of Part 1: the cardiac-gating and DWI 13

2.3.1 The acquisition of cardiac-gating DWI 13

2.3.2 Post-process in MRI data 13

2.3.3 Motion artifacts 13

2.3.4 Diffusion tensor parameters 14

2.3.5 TBSS analysis 15

2.3.6 V1 direction comparison 15

2.3.7 Fiber tractography in CST 16

2.3.8 Tract variability analysis with Jaccard Distance 16

2.3.9 Statistics analysis 17

2.4 Methods in study of Part 2: the denoising algorithm POAS and DWI 17

2.4.1 DWI post-processing and POAS denoising 17

2.4.2 Image inspection and SNR evaluation 17

2.4.3 FA and MD value comparison with TBSS analysis 18

2.4.4 Variability analysis of DWI intensity and FA value in original and POAS-processed data 19

2.4.5 Tractography of corticospinal tract and tract profile analysis 19

2.4.7 Reproducibility and similarity analysis of corticospinal tract 20
2.4.8 Statistical analysis 21
3. RESULTS 22
3.1 Results of part 1: cardiac gating and DWI *22*
3.1.1 DWI motion artifacts and signal variability 22
3.1.2 Diffusion tensor parameters analysis 24
3.1.3 TBSS analysis 25
3.1.4 Principal eigenvector analysis 27
3.1.5 Tractography in the CST 27
3.1.6 Analysis of the tract variability 28
3.2 Results of part 2: POAS and DWI *29*
3.2.1 Inspection of the DWI images and estimation of the SNR 29
3.2.2 TBSS analysis of the FA and MD values 30
3.2.3 Variability assessment of DWI and FA 32
3.2.4 Tractography of the CST 33
3.2.5 Tract profile of CST 33
3.2.6 Reproducibility and similarity of the analysis of the CST 35
4. DISCUSSION 37
4.1 Discussion of Part 1: cardiac-gating and DWI *37*
4.2 Discussion of Part 2: POAS and DWI *42*
4.3 General discussion of both parts *48*
5. SUMMARY 51
6. ZUSAMMENFASSUNG 53
7. REFERENCE 55
CURRICULUM VITAE 64
PUBLICATION 65
LIST OF ACADEMIC TEACHERS 66
ACKNOWLEDGEMENT 67

Abbreviation

MPRAGE: magnetization-prepared rapid acquisition with gradient echo

DWI: diffusion weighted imaging

DTI: diffusion tensor imaging

SNR: signal to noise ratio

CST: corticospinal tract

BS: brain stem

PLIC: posterior limb of internal capsule

ALIC: anterior limb of internal capsule

SC: subcortex

CC: corpus callosum

POAS: position-orientation adaptive smoothing

TBSS: tract based spatial statistics

List of Figures

Fig.1: the color-coded FA map

Fig.2: the ROIs indication for SNR calculation

Fig.3: visual inspection of DWIs in single volunteers

Fig.4: standard deviation (SD) differences across non-gating and cardiac-gating data

Fig.5: analysis of FA and MD within the masked CST

Fig.6: the TBSS analysis in diffusion tensor parameters including FA, MD, and eigenvalues L1, L2 and L3.

Fig.7: the TBSS analysis of principal eigenvector (V1)

Fig.8: the slice analysis in principal eigenvector (V1)

Fig.9: fiber tractography of CST in one participant

Fig.10: the DWIs from original, POAS-processed, and averaged datasets

Fig.11: TBSS analysis of whole brain in FA and MD value

Fig.12: the difference-CV map and the relative histogram graph in DWI intensity and FA value

Fig.13: the tractography of CST in one volunteer

Fig.14: the illustration of tract volume and fiber density in CST

List of Tables

Table 1: the change of diffusion tensor parameters after cardiac-gating

Table 2: tract volume and Jaccard distance (JD) along CST and its subdivisions (BS, PLIC, and SC) between non-gating (NG) and cardiac-gating (G) group

Table 3: tract profile of CST including fiber volume, FA value, MD value and fiber density

Table 4: results of reproducibility and similarity analysis evaluated with Jaccard index

Table 5: the comparison between the effect of cardiac-gating and POAS

1. Introduction

1.1 Background: Diffusion weighted imaging, diffusion tensor imaging, and tractography

Diffusion tensor imaging (DTI) has become a very popular technique in the clinic, and has been applied in many different kinds of studies and subjects. It is usually used to reconstruct white matter tracts to guide neurosurgery. The white matter of the brain is composed of complex structures. Typically, fiber bundles with similar directions have similar functions, therefore, by analyzing the pathways of these fibers it is possible to investigate the structure and function of different brain regions. However, because of the enormous variation in brain structures, previous studies based on post-mortem brains were therefore unable to study individuals in vivo. Therefore, diffusion tensor imaging, an approach based on the measurement of the diffusion coefficient in random directions, allowed the non-invasive visualization of white matter tracts. In 1905, Einstein described the calculation of the diffusion coefficient in free conditions (*Einstein 1905*). The diffusion coefficient is associated with the molecular size, temperature, and the viscosity of the medium. Commonly, in a homogeneous medium, the thermal movement of water molecules, also known as Brownian motion, follows a Gaussian distribution, and the displacement of the molecular diffusion in a random direction is always the same based on Einstein's description, which is called isotropic diffusion. However, in a non-homogenous medium, the diffusion displacement of water molecules becomes entirely different in a random direction. This phenomenon is called anisotropic diffusion. For example, in the tissues of the muscles and the brain, there are dense fibers with coherent orientations, and water molecules tend to diffuse along these fibers. So the diffusion coefficient becomes the largest when diffusion is measured along the fibers, while it is the smallest when in a perpendicular direction which is obscured. Then, the direction with the largest diffusion coefficient will indicate the orientation of the white matter fibers. The white matter of the brain is made up of complex fiber bundles. Therefore, based on the anisotropic diffusion of the water molecules, we can map out the directions of fiber

bundles.

Dr. Stejskal and Tanner introduced a method to calculate the diffusion coefficient in random directions using nuclear magnetic resonance and magnetic resonance gradient systems (*Stejskal, Tanner 1965*). With this, we can non-invasively depict the structure of the white matter of the brain by calculating the diffusion anisotropy using MRI. This MRI technique is called diffusion MRI. Ideally, acquisition from infinite gradient directions should lead to the precise estimation of the diffusion anisotropy so that the actual fiber structures of the white matter can be determined. However, the acquisition time is always the limiting factor in the clinical setting. Therefore, it is important to determine how many gradient directions are sufficient to make a rather accurate estimation. In the early 1990s, a tensor model emerged (*Basser et al. 1994a, b,Mori, Barker 1999*), called diffusion tensor imaging (DTI). The tensor model introduced the concept indicating that the diffusion anisotropy could be simulated with an ellipsoid. To define an ellipsoid, at least six parameters are needed, six measurements of lengths along six arbitrary axes. Hence, the DTI needs at least seven diffusion volumes including one diffusion non-weighted image and six diffusion weighted images in six arbitrary gradient directions. Of course, acquisition with more gradient directions may indicate, more precisely, the orientation of the diffusion anisotropy. There is a study reported that at least 20 unique gradient directions are necessary for a robust estimation of anisotropy, and at least 30 gradient directions are essential for a robust estimation of tensor-orientation and mean diffusivity (*Jones 2004*).

The tensor model mimics an ellipsoid, which produces six parameters, the shortest and longest lengths and the middle axes which are perpendicular to each other, and their respective directions. Lengths with eigenvalues are represented by λ_1, λ_2, and λ_3, and their directions are represented by vectors, named eigenvectors V1, V2, and V_3. According to these parameters, anisotropy and diffusivity are usually calculated by using the fractional anisotropy (FA) and mean diffusivity (MD), respectively.

$$\mathrm{FA} = \sqrt{\frac{1}{2}} \frac{\sqrt{(\lambda_1 - \lambda_2)^2 + (\lambda_2 - \lambda_3)^2 + (\lambda_3 - \lambda_1)^2}}{\sqrt{\lambda_1^2 + \lambda_2^2 + \lambda_3^2}}$$

$$\mathrm{MD} = (\lambda_1 + \lambda_2 + \lambda_3)/3$$

The color map of the FA may indicate the orientation of the fiber bundles (Fig.1). Based on the FA map, the fiber tract may be reconstructed in three dimensions after defining the region of interests (ROIs) of inclusion and exclusion. Fibers through the ROIs of inclusion and not in the ROIs of exclusion represent the target tracts.

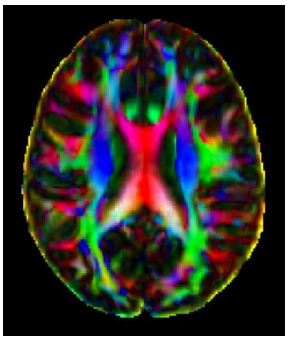

Fig.1: A color-coded map of FA. Red represents the fibers running in the right-left direction; green, anterior-posterior direction; and blue, superior-inferior direction.

1.2 Application of the DWI and DTI in neuroscience

Since the diffusion characteristics of water are dependent on the composition and architecture of a biological environment, quantified maps of diffusion parameters, such as FA and MD, may demonstrate any change in the microstructures and help to diagnose neurological diseases. Diffusion MRI has been used in cases of brain strokes (*Madai et al. 2014,Warach et al. 1995*), neurodegenerative diseases (*Rizzo et al. 2008,Yoshiura et al. 2003*), traumatic brain injury and aneurysmal subarachnoid hemorrhage (*Sener et al. 2016*), infectious diseases (*Guo et al. 2001*), and intracranial tumor grading (*Federau et al. 2014,Wu et al. 2012*), by measuring the changes in the diffusion tensor parameters in different tissues. Recently, the quantitative and automatic segmentation of brain tumors has been conducted according to the diffusion tensor parameters, such as the apparent diffusion coefficient (ADC) (*Scherer et al. 2018*). Diffusion MRI is currently the only approach used to non-invasively map white matter connectivity in vivo by measuring the random coherent motion of water molecules (*Basser et al. 2000,Jones et al. 2013,Mori et al. 1999*). Based on the diffusion tensor model, DTI has attracted much attention for the delineation of the white matter tracts in vivo (*Basser et al. 2000,Mori et al. 1999*), which is helpful in guiding resections during surgery and for

predicting neurologic function after surgery (*Bello et al. 2008,Murakami et al. 2008,Nimsky et al. 2005a, b,Nimsky et al. 2006,Yamada et al. 2003*). The growing interest in DWI and DTI has made it essential to consider what factors affect the quality of the acquisition and the accuracy of the diffusion metrics as well as the accuracy of white matter reconstruction.

1.3 Disadvantages of DWI

Compared to conventional MRI, such as T1 and T2, DWI has many disadvantages (*Le Bihan et al. 2006*). First, DWI is relatively motion-sensitive because it measures the diffusion movement of water molecules. So the use of DWI often results in more artifacts coming from the bulk motions and physiological motions. Normally, fast scanning is a method used to reduce the risk of motion artifacts. However, for DTI acquisition, more diffusion gradients help to acquire more precise and stable results, which of course needs more acquisition time. And this will definitely be in higher chance to produce motion artifacts. Second, scanning of DWI requires a strong diffusion gradient field. The stronger the diffusion gradient field is, the more information about the diffusion characteristics we can get from DWI. But more signal suppression with obvious artifacts will be made and it hinders the image quality. At the same time, most of DWIs are acquired with echo planar imaging sequence, which is more easily suffered from eddy current and geometric distortion. Therefore, DWIs always have a low SNR and image distortion. Given these disadvantages, modification during acquisition and some post-processing approaches have been proposed to improve image quality, which is important for subsequent analyses and reconstruction.

1.4 Objectives of this study

Since tractography has played an important role in neurosurgery and DWI is the basis of it, good quality of DWI acquisition is necessary. In this study, we investigated two approaches, cardiac-gating and a denoising approach named position-orientation adaptive smoothing (POAS) on the optimization of DWI. These two approaches may decrease the artifacts and improve the image quality from different aspects. Therefore, our study included two parts, the effect of cardiac-gating and that of POAS, respectively.

1.5 Background and objectives of part 1

Measurement of the Brownian motion of water molecules is the principle of DWI. Brownian motion is a kind of micro-motion with a displacement of 10 μm/50 ms (normal diffusion-encoding time) (*Habib et al. 2010*). In the brain, besides this micro-motion, there still exists bulk motion during an MRI scanning, such as head movement and brain physiological pulsatile motion. Head movement is a patient's voluntary movement and can be eliminated by using head pads to keep the head stable during an MRI scanning. Pulsatile motion in the brain occurs during the cardiac systolic period and is motivated by arterial pulse, venous expansion, cerebral spinal fluid (CSF) flow and capillary expansion (*Kan et al. 2014*). Cerebral artery pulse is the primary power for pulsatile motion (*Greitz et al. 1992*). It has been reported that brain pulsatile motion has a displacement of 100-184 μm/50 ms (*Habib et al. 2010,Nunes et al. 2005*). It is much larger when compared to Brownian motion. The highest velocities occur in the brain stem (1.5 mm/s) with a caudal-anterior direction, and the basal ganglia (1.0 mm/s) with a caudal medial-posterior direction (*Greitz et al. 1992*). In T1 and T2 acquisition, pulsatile motion artifacts are normally not visible except in some pathological situations, like a normal pressure hydrocephalus and a Chiari I malformation (*Kan et al. 2015,Radmanesh et al. 2015*). However, since DWI is sensitive to Brownian motion, the pulsatile motion of the brain which has a larger movement than Brownian motion might influence DWI. Moreover, in order to decrease the influence of pulsatile motion during the systolic period, cardiac-gating has been suggested via acquisition of the MRI signal only in the diastolic period (*Lenz et al. 1989,Skare, Andersson 2001*).

To date, there is still debate regarding the exact influence of pulsatile motion and function of cardiac-gating. Some researchers reported prominent signal artifacts in non-gated DWIs. In these studies, cardiac-gating resulted in the elimination of the motion artifacts (*Pierpaoli et al. 2003*). However, some studies found that this pulsatile motion effect was less pronounced when the motion artifacts were only approximately 6%–20% (*Nunes et al. 2005,Skare, Andersson 2001*). Some researchers detected no apparent artifacts, and found no improvement after cardiac-gating (*Nagy et al. 2008*). Several reports which considered cardiac-gating to be

helpful demonstrated that cardiac-gated DWIs had fewer artifacts and less bias in diffusion tensor parameters, such as FA and MD (*Habib et al. 2008,Habib et al. 2009,Habib et al. 2010,Kim et al. 2010,Pierpaoli et al. 2003,Skare, Andersson 2001*). Moreover, other studies showed a deviation of the direction of the principal eigenvector due to pulsatile motion (*Kozák et al. 2013,Walker et al. 2011*). However, only one article reported the effects of pulsatile motion on white matter tractography, mainly on the corpus callosum and the fornix (*Jones, Pierpaoli 2005*). Although some evidence for the advantages of cardiac-gating exist, it is not usually considered in clinical settings because the acquisition time with cardiac-gating is variable depending on the heart rate and can become quite long. This is associated with an increased risk of more head movements (*Nunes et al. 2005*).

Based on previous reports, the most obvious pulsatile motion occurred in the brain stem and the basal ganglia, therefore the corticospinal tract passing through these regions may be affected more easily. The CST is an important white matter fiber bundle in neurosurgery responsible for limb movement. In this first part of the study, we aimed to determine the influence of pulsatile motion on CST, and the effect of cardiac-gating on motion artifacts, diffusion tensor parameters and the tractography of the CST.

1.6 Background and objectives of part 2

Compared with other imaging modalities whose quality is easily affected by scanner parameters and subject motion (*Gao et al. 2009,Polders et al. 2011,Walker et al. 2011,Wang et al. 2012*), DWI suffers more from its inherent challenges. It is often limited to a low spatial resolution and adverse effects like blurring, localized signal loss and image distortions (*Bammer et al. 2009*). Influenced by these drawbacks, the analysis of DWI can be erroneous which may lead to incorrect medical decisions. High quality DWI requires both a high spatial resolution and a high angular resolution (*Zhan et al. 2013*). The smaller size of the voxels contributes to a higher spatial resolution, and more diffusion gradients and larger b values produce a higher angular resolution. The angular resolution affects the reliability of the diffusion measures (*Zhan et al. 2010*) as well as the stability and the complexity of the fiber tractography (*Calabrese et al. 2014,Jones 2004,Tuch 1999*). High angular resolution diffusion

imaging (HARDI) is an excellent example of tracking crossing or intermixing of white matter tracts in the brain (*Tuch et al. 2002,Tuch 2004*). However, it requires a much longer acquisition time and is therefore not used in a clinical setting. Moreover, larger b values in HARDI lead to a lower signal to noise ratio (SNR) which damages the image quality (*Xie et al. 2015*). Higher spatial resolution is necessary for differentiation of neighboring tissues and helps to more accurately depict the diffusion properties. However, except for sacrificing with longer acquisition time, a higher resolution is also inherently companied with a lower SNR, which decreases the reliability and accuracy of the fiber tracts (*Jones, Basser 2004,Kim et al. 2006*). As a result, balancing both SNR and spatial resolution as well as improving angular resolution is the best solution to obtain high-quality results from DWI.

In brain MRIs, the achievable SNR is affected by motion, susceptibility-related distortions, physiological effects, and even scan duration (*Xie et al. 2015*). Improvement of the SNR relies on two solutions: increasing acquisition time by averaging the repeated scans (*Holmes et al. 1998*), or post-processing which is time-saving and quite effective. The limitation of acquisition time in clinics is a common problem because of the patients' conditions. Therefore, post-processing is usually the recommended approach to improve SNR. Some denoising approaches have been proposed to enhance the image quality and preserve SNR, such as Gaussian filtering (*Westin et al. 1999*), wavelet transformation (*Wirestam et al. 2006*), Perona-Malik filter (*Perona, Malik 1990*), non-linear anisotropic diffusion filter (*Weickert 1998*), the propagation-Separation approach (*Polzehl, Spokoiny 2006*), nonlocal means (*Wiest-Daesslé et al. 2008*), linear minimum mean square error estimation (*Aja-Fernández et al. 2008*), and local principal component analysis (*Manjón et al. 2013*). Notably, in a diagnostic image, preservation of the edge when reducing the noise is quite crucial for the maintenance of the original clinical significance (*Mohan et al. 2014*). There have been many associated approaches reported and position-orientation adaptive smoothing (POAS) is a sophisticated smoothing way for noise reduction among them (*Becker et al. 2012,Becker et al. 2014*). For diffusion data enhancement, this technique requires structural adaptive smoothing in both voxel space and diffusion gradient space. Smoothing in voxel and diffusion gradient

space is embedded in an iterative adaptive multi-scale approach. The adaptive character avoids blurring of the internal structures and preserves discontinuities. POAS does not rely on a specific model such as the diffusion tensor model or higher order models so it can be applied widely. This technique has been reported to allow edge-preservation and avoid blurring of the fine anisotropic structures in DWI, which has produced comparable effect with other denoising algorithms such as non-local means and joint denoising (*Becker et al. 2012,Becker et al. 2014*).

In part 2 of this study, we investigated the contribution of POAS in the improvement of SNR and the compensation effect of spatial resolution and angular resolution in DWI. With the use of POAS to reduce noise, first, we verified whether there was a noticeable improvement of the image quality in DWI, such as SNR, to compensate for the drawbacks caused by the spatial resolution. Then, we detected the change in the diffusion metrics such as FA and MD and estimated the variability of the DWI signal and the FA value. Finally, we estimated the effects of POAS in fiber tractography of corticospinal tract (CST) to determine if it could compensate for the limitations of angular resolution. Because average is a conventional method to improve SNR and enhance the image quality (*Holmes et al. 1998*), we also evaluated the difference between the effect of POAS and the average to clarify if POAS could compensate for the effects of multiple averages and help to save the acquisition time.

2. Materials and Methods

2.1 Participants

This prospective project was approved by the Ethics Committee in Philipps University in Marburg, Germany, and based on the declaration of Helsinki (*Association 2001*). Informed written consent was obtained from every participant. There were 22 healthy volunteers without known history of disease in our study, including 9 males and 13 females. The average age was 27.45±6.10 years old (from 22 to 49).

2.2 MRI acquisition

All MRI datasets in this study were performed on 3.0 Tesla scanners (Trio Tim, Siemens, Erlangen, Germany) using a 12-multichannel receiver head coil. During the scanning, the participants were in supine position and their heads were fixed with soft foam rubber pads to minimize head bulk motion. The volunteers all received the standard T1-MPRAGE, T2 and DWI acquisition.

The setting of parameters in T1-MPRAGE is: slice thickness 1mm, field of view (FOV) 256×256mm, 176 slices, time of repetition (TR) 1900ms, time of echo (TE) 2.26ms, bandwidth 200Hz, PAT mode GRAPPA with accelerate factor 2.

The setting of parameters in T2WI is: slice thickness 1mm, FOV 256×256mm, 176 slices, TR 3200ms, TE 402ms, bandwidth 752Hz, PAT mode GRAPPA with accelerate factor 2.

The setting of parameters in DWI is: slice thickness 2mm, FOV 256×256mm, 60 slices without slice gap, TR 7800ms, TE 90ms, orientation transversal, phase encoding direction anterior >> posterior, b value 1000s/mm^2, diffusion directions 30 in arbitrary non-collinear directions, 7 B0 images acquired after every five diffusion weighted gradient images, bandwidth 1502Hz, phase partial Fourier 6/8. Each volunteer received the DWI acquisitions five times continuously with same parameters. Then the acquisition which had obvious artifacts or distortion would be excluded from the further analysis.

2.3 Methods in study of Part 1: the cardiac-gating and DWI

2.3.1 The acquisition of cardiac-gating DWI

With cardiac-gating, the TR in DWI became variable according to the connected heart rate. So for non-gating DWI, the TR was set to 7800ms and for the cardiac-gating DWI TR was varied around 700ms. The cardiac gating was conducted based on peripheral pulse. Non-gating DWI scanning took about 6 minutes and cardiac-gating DWI acquisition took about 10 minutes. In the study about cardiac gating and DWI, each volunteer also received the cardiac-gating DWIs five times continuously with same setting. The acquisition with obvious artifacts or distortion was excluded.

2.3.2 Post-process in MRI data

First, non-gating and cardiac-gating DWIs were all corrected for bulk motion and eddy current distortions in FSL (FMRIB Software Library, Oxford, UK) with the tool "eddy". Diffusion tensors were estimated and the maps of diffusion tensor parameters, such as FA, MD, three eigenvalues L1, L2, L3 and principal eigenvector V1 were created with the tool "dtifit" in FSL with default parameters. Then the datasets for analysis were registered to MNI152 (Montreal Neurological Institute) space with FLIRT (FMRIB's Linear Image Registration Tool, Oxford, UK) and FNIRT (FMRIB's Non-Linear Image Registration Tool, Oxford, UK) transformation. The scheme of registration was followed: 1) subject's original T1 was registered to MNI152_1mm standard-space T1 template with both FLIRT and FNIRT transformation, and got the transformation matrix; 2) B_0 image was registered to the original T1, with FLIRT transformation, and got the transformation matrix; 3) applying both matrixes produced in previous two steps to the images which need to be registered to MNI152 standard space, like DWI, FA, MD or eigenvalue maps L1, L2, L3, V1.

2.3.3 Motion artifacts

In order to evaluate motion artifacts, each DWI acquisition was checked volume by volume. Normally, when the gradient direction is the same with the direction of pulsatile motion, there will be the most obvious motion artifacts (*Greitz et al. 1992,Nunes et al. 2005*). Previous

researches demonstrated when gradient direction was along with Z axis, prominent artifacts could be observed in brain stem and cerebellum (*Chung et al. 2010,Habib et al. 2010,Skare, Andersson 2001*). This result might have the prerequisite that brain stem was proximately parallel to Z axis. We calculated the subspace angle from gradient direction to Z axis (the cosine of the subspace angle equals the dot product of diffusion encoding gradient direction and Z axis divided by the product of their vector magnitudes). Among the 30 diffusion weighted gradient directions in each DWI acquisition, the volume with smallest subspace angle closer to $0°$ (in this study with $18.77° \pm 5.42°$ on average, diffusion weighted gradient direction #24, named volume 24 in the following paragraphs) and the volume with biggest subspace angle closer to $90°$ (in this study with $95.52° \pm 2.35°$ on average, diffusion weighted gradient direction #17, named volume 17 in following paragraphs) were selected. So in each volunteer, we separately compared the volume 24 and volume 17 between the five repetitive non-gating and five cardiac-gating DWI acquisitions. The pulsatile motion artifacts were estimated by comparing difference of the signal intensity between non-gating and cardiac-gating DWIs. According to previous reports, the signal loss or signal attenuation was regarded as obvious pulsatile motion artifacts (*Habib et al. 2010*). Then we also averaged the five repetitive non-gating and cardiac-gating DWIs and got the averaged non-gating and cardiac-gating datasets separately. The averaged datasets were also compared with the individual datasets aforementioned to see the effect of average.

In order to know which part of brain had more obvious variation in DWI signal intensity, standard deviation (SD) maps, which were from the five non-gating or five cardiac-gating DWIs in each volunteer, were created in Matlab R2017a (Mathworks Inc., Natick MA, USA) with self-written scripts.

2.3.4 Diffusion tensor parameters

Diffusion tensor parameters, including FA and MD, were calculated and analyzed in the datasets which had been registered to MNI152 standard space. First, the general analysis in diffusion tensor parameters was conducted in the region of whole corticospinal tract (CST) between non-gating and cardiac-gating datasets. The mask of whole CST was made based on

JHU white matter tractography atlas in FSL. The values of diffusion tensor parameters in the mask in each DWI acquisition were calculated with *fslmeants* in FSL. Then the average values of each diffusion tensor parameter among the five non-gating datasets or among five cardiac-gating datasets were calculated separately in each volunteer for further comparison. Second, in order to know which part of CST got more obvious difference in diffusion tensor parameters between non-gating and cardiac-gating datasets, we also did the slice analysis. From pons to motor cortex of CST, we made the slice masks for every 5 mm and calculated the FA and MD values in every slice.

2.3.5 TBSS analysis

In order to know the voxel-wise difference of diffusion tensor parameters, the TBSS (tract based spatial statistics) analysis was carried out (*Smith et al. 2006*). First, all subjects' FA data was aligned with FMRIB58_FA standard-space FA template in MNI152 standard space. The co-registration was done with nonlinear transformations. Then all subjects' aligned FA data were projected to FMRIB58_FA mean FA image and were merged into a single file. The voxel-wise analysis across the non-gating and cardiac-gating group was carried out with threshold $FA \geq 0.20$ to exclude peripheral tracts. The results were tested using permutation-based statistical analysis with 500 permutations and were corrected using threshold-free cluster enhancement (TFCE) method. The significance level was set to $p<0.05$. Moreover, to know the analysis about MD, L1, L2 and L3, their maps were transformed accordingly, projected on FA skeleton and processed similar with the FA data.

2.3.6 V1 direction comparison

To evaluate the direction change of principal eigenvector which was affected by pulsatile motion, the voxel-wise analysis in V1 map between non-gating and cardiac-gating was carried on. Because the CST roughly followed Z axis, the V1 map in Z axis was separated from the original V1 map created in FSL. The angle between the principal eigenvector V1 and Z axis (see calculation in subspace angle in 2.3.3) was calculated as voxel value and the resulting map was used in the following analysis. The voxel-wise analysis was conducted

with TBSS using non-FA steps aforementioned. We also did the slice analysis in V1 (5mm as a slice, same with the slice analysis in diffusion tensor parameters introduced above) between non-gating and cardiac-gating group to estimate the angle difference of principal eigenvector in different part of CST.

2.3.7 Fiber tractography in CST

Fiber tracking on CST was carried out with streamline approach in iPlan software (Brainlab, Feldkirchen, Germany). Two included regions, cerebral peduncle and motor cortex, were drawn manually in T1 images for CST tractography and we excluded the fibers not belonging to CST. Then the volume of whole CST was acquired in each DWI dataset. The generated CSTs in either side in each volunteer were output for further analysis in morphology.

2.3.8 Tract variability analysis with Jaccard Distance

Among the five repetitive non-gating or cardiac-gating CSTs which were output previously, Jaccard distance was calculated to evaluate the individual variability among CSTs in either group.

$$JD=1-\frac{\text{intersection volume}}{\text{union volume}}$$

The intersection volume and union volume was calculated with Mevislab (http://www.mevislab.de/). The idea of Jaccard distance (JD) came from Jaccard index (JI). The JI measured with intersection size divided by union size is a normalized evaluation of overlap between two samples (*Glozman et al. 2018,Jaccard 1901*). Based on the idea of JI, the JD could be used to represent the difference and variation of tracts in this study.

In every volunteer, we got the volume of intersection part and union part among either five non-gating or five cardiac-gating CSTs and calculated the JD value in both groups separately. Then we divided CST into three parts, brain stem part (BS), internal capsule of posterior limb(PLIC) part and the part above corpus callosum (subcortex, SC) according to anatomy. And we calculated the JD value in each part.

2.3.9 Statistics analysis

Statistical analysis was conducted in SPSS Statistics 24.0 (IBM, Armonk, USA) with either independent student t-test or paired t-test. Statistical significance was accepted only with $P<0.05$.

2.4 Methods in study of Part 2: the denoising algorithm POAS and DWI

2.4.1 DWI post-processing and POAS denoising

First, the raw DWI data (aforementioned in section 2.2) was corrected for motion and eddy current distortions in FSL (FMRIB Software Library, Oxford, UK). Then the corrected DWI data was denoised with algorithm POAS using POAS4SPM toolbox in part of ACID toolbox (artifact correction in diffusion MRI, http://www.diffusiontools.com/) in SPM (statistical parametric mapping) platform (*Penny et al. 2011*). The associated parameters of POAS were as follows: L=2, sigma=70, lambda=12, K star=12, Kappa=0.8. All the parameters were decided based on the reported study (*Tabelow et al. 2015*) and the actual DWI scanning parameters within our scanner. For each DWI acquisition, the processing of POAS took about 40min on our PC (Windows 10 operation system, Intel(R) Core(TM) i5 CPU, 2.40GHZ, 12GB RAM).

2.4.2 Image inspection and SNR evaluation

In order to know the denoising effect produced by POAS, image inspection was conducted among the original DWI data, POAS-processed data and also the averaged data. The original DWI data was without POAS denoising process, while the averaged data in each volunteer was from the averaging of the five repetitively original DWI acquisitions. All the DWI data in each group received same process and analysis in the following methods.

Except for the qualitative inspection in image quality, the quantitative comparison was carried on with the estimation of SNR. The SNR calculation was conducted in the same ROIs among original, POAS-processed and averaged data. First, all DWI images from these three groups were normalized to MNI152 standard space. The SNR equaled to the mean value of signal

intensity divided by the sample standard deviation of noise intensity in diffusion non-weighted images (B0 images). Because there were 7 B0 images in a single DWI acquisition, first we got the averaged B0 image for the calculation of SNR. The ROI for signal intensity was chosen in a stable anatomical structure with clear contrast, for example corpus callosum. So the mask of corpus callosum was set as the ROI for calculation the mean signal intensity value (Fig. 2A). The ROI for noise signal intensity should come from the background noise. So four random selected $1 \times 1 \times 1$ cm^3 cubes was made in the location of background to calculate the standard deviation of noise signal intensity in averaged B0 image (Fig. 2B).

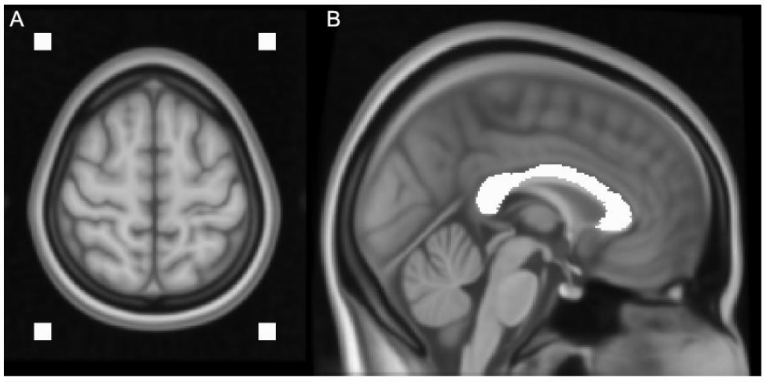

Fig.2: the ROIs indication for SNR calculation. A: these four dotted ROIs in the background were used for the calculation of noise; B: the ROI in corpus callosum was used for the calculation of signal.

2.4.3 FA and MD value comparison with TBSS analysis

In order to assess the influence of POAS in diffusion tensor parameters, we conducted TBSS analysis to evaluate the difference of FA and MD value among original, POAS-processed and averaged data (*Smith et al. 2006*). With the *dtifit* in FSL, the FA maps were acquired through standard linear regression. First, all FA maps were normalized to the standard MNI space using non-linear registration (*Rueckert et al. 1999*) and all transformed data sets were subsequently resampled, resulting in a spatial resolution of 1x1x1mm ³. Then, all aligned FA data sets were projected onto the template FMRIB58_FA standard-space FA image using a non-maximum suppression threshold of FA≥0.20. The resulting data was fed into the voxel-wise analysis. The comparison was set up with general linear model (GLM) in FSL(*Nichols, Holmes 2002,Winkler et al. 2014*). The model of tripled t-test was applied with

three contrasts separately, original vs. POAS-processed data, original vs. averaged data, and POAS-processed vs. averaged data. Three contrasts were analyzed according to permutation-based non-parametric inference with 500 random permutations using threshold-free cluster enhancement (TFCE) (*Smith, Nichols 2009*) to correct for multiple testing. Significance level was set to $p<0.05$. The TBSS analysis of MD value was conducted as the pipeline of non-FA method accordingly. The comparison of MD value among three groups was performed in the same way with FA value as aforementioned.

2.4.4 Variability analysis of DWI intensity and FA value in original and POAS-processed data

In each volunteer, the variability of DWI intensity and FA value among five repeated DWI or FA images was assessed by the coefficient of variation (CV). And the CV separately in original data (CV-origin) and POAS-processed data (CV-POAS) was compared. First, the SD map and average map in each volunteer were calculated among these five repetitive DWI or FA maps. Then the CV map was acquired with SD map divided by average map. Finally, the difference-CV map, which was CV-POAS map subtracted from CV-origin map, was inspected for variability assessment between original and POAS-processed data. The histogram of difference-CV map was used for the distribution demonstration of the difference CV value.

2.4.5 Tractography of corticospinal tract and tract profile analysis

To estimate the effect of POAS in fiber tractography, corticospinal tract (CST) was reconstructed. The fiber tracking was done automatically with AFQ (automated fiber quantification) software (Vista Lab, Stanford University, USA) (*Yeatman et al. 2012*) to eliminate the manual bias (*O'Donnell et al. 2017,Zhang et al. 2008*). First, whole brain tractography with deterministic FACT algorithm was conducted and then segmentation for fiber groups, including CST, was carried on using defined standard template of ROIs (*Zhang et al. 2008*). The standard ROIs came from MNI-JHU-tracts-ROI and the ROIs were then transformed to the subject data. Because all the subject data from these three groups had already been normalized to MNI152 standard space before tractography, the ROIs after

transformation would also be in MNI152 standard space. Finally the produced CSTs were also in MNI152 standard space. The eliminating of unrelated fibers was based on the tract probability map, and the fibers who didn't pass through it would be removed (*Hua et al. 2008*). Analysis was carried on the automatically produced CSTs. The volume of CST in all of three groups was calculated based on the number of voxels ($1ml/10^3$ voxels). The mean FA value of CST, and mean MD value was also acquired in AFQ software. The fiber density of CST which was calculated with the streamline counts divided by fiber volume was also acquired. The comparison of fiber volume, fiber density, FA and MD value in CST among these three groups was conducted as tract profile. In the averaged data, except for deterministic FACT algorithm aforementioned, the algorithm of constrained spherical deconvolution (CSD) was also performed as a standard reference for CST evaluation (CST-reference), because the CSD could better reconstruct white matter with higher complexity and reliability (*Auriat et al. 2015,Tournier et al. 2007,Tournier et al. 2008*).

2.4.7 Reproducibility and similarity analysis of corticospinal tract

Because in each volunteer there were five original and five POAS-processed DWI data sets, five CSTs from original data (CST-origin) and five CSTs from POAS-processed data (CST-POAS) were acquired. The reproducibility among the five CST-origins or among the five CST-POASs was analyzed respectively to estimate the effect of POAS on tractography. Jaccard index (JI) was to indicate the degree of similarity which referred to the reproducibility here for CSTs. The JI was defined as the volume of intersection part divided by the volume of union part (*Glozman et al. 2018,Jaccard 1901*). So the JI here could reflect the reproducibility not only in volume of CST but also in location and shape of CST generally.

Then we analyzed the similarity between CST-origin and CST-POAS group. Each CST-origin had a relevant CST-POAS, so we calculated the JI between them to identify the similarity. The similarity analysis in CST-origin vs. CST-reference and CST-POAS vs. CST-reference were also estimated with JI respectively.

2.4.8 Statistical analysis

The results of continuous variables were described as mean ± SD. Shapiro-Wilk test was used for testing normal distribution. When normal distribution was met, randomized block design in analysis of variance (ANOVA) was performed to compare the difference among original, POAS-processed and averaged data. Group and volunteer were regarded as the fixed factors. Then the pairwise comparison separately in original vs. POAS-processed, original vs. averaged, POAS-processed vs. averaged data were conducted with Tukey's HSD test. When we evaluated the reproducibility between the CST-origins and CST-POASs, paired t-test was performed to verify the significant difference. When normal distribution was not met, the Wilcoxon signed-rank test was conducted for the comparison between two related groups. In this study, the statistical significance was accepted only when P value <0.05.

3. Results

3.1 Results of part 1: cardiac gating and DWI

3.1.1 DWI motion artifacts and signal variability

In volume 24, which had the smallest subspace angle from the current gradient direction to the Z axis, obvious artifacts could be found in the superior cerebellum and the mesencephalon in thirteen volunteers out of the twenty-two volunteers in non-gating DWIs (Fig.3A, B). Also, among the five repetitive non-gating DWIs, motion artifacts occurred randomly and were normally observed only in one of the five DWIs. There was not any prominent signal loss or signal attenuation regarded as pulsatile motion artifacts in cardiac-gating DWIs. Therefore, the artifacts occurrence ratio in the non-gating data was about 11.82%, which was calculated as the number of datasets with signal alterations (13×1) divided by the total number of datasets (22×5). In volume 17 which had a subspace angle closer to 90 °, five volunteers were found with obvious signal artifacts in the mesencephalon (Fig.3C), therefore, the artifacts occurrence ratio was about 4.55%. After image averaging of the repeated acquisitions, the artifacts in the non-gated group almost disappeared. Analysis of the SD maps demonstrated that two regions, the mesencephalon and superior cerebellum, presented obviously higher SD values in the non-gated group than the gated group (Fig. 4).

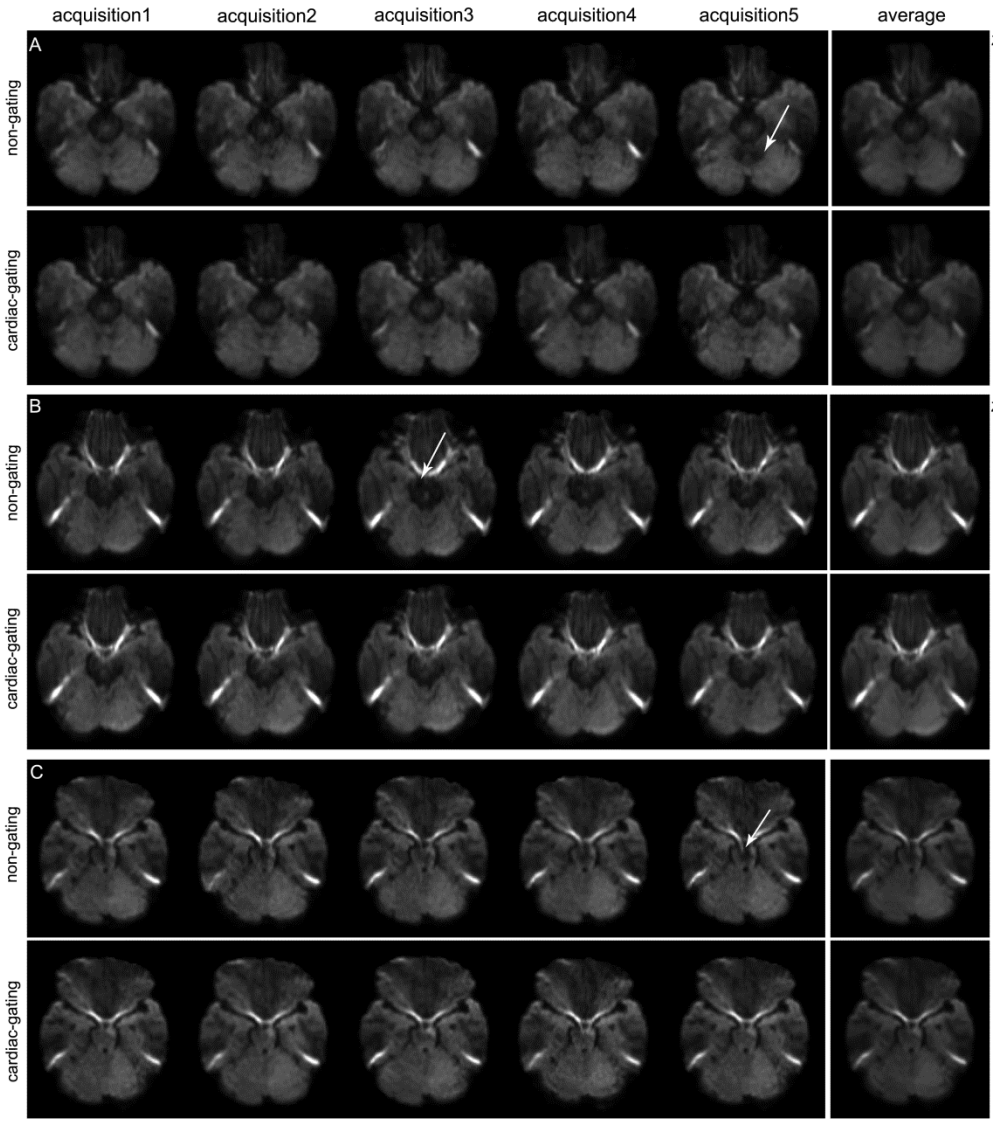

Fig.3：Visual inspection of the DWIs in a single volunteer. Pulsatile motion artifacts (which had an obvious signal loss or attenuation) were observed only in the non-gated group, while in the averaged and cardiac-gated images, the artifacts were invisible. A: DWIs in volume 24 with the smallest deviation from the Z-axis (the white arrow shows an obvious pulsatile motion artifact in the superior cerebellum only in the non-gated DWIs); B: DWIs in volume 24 with the smallest deviation from the Z-axis (the white arrow shows pulsatile motion artifacts in the brain stem only in the non-gated DWIs); C: DWIs in volume 17 with a 90 °deviation from the Z-axis (the white arrow shows pulsatile motion in the brain stem).

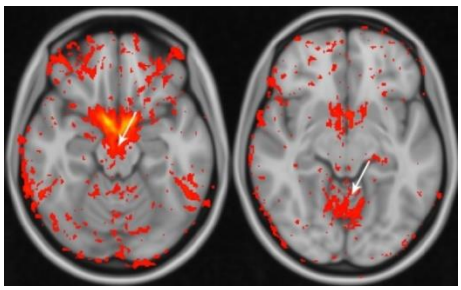

Fig.4: Standard deviation (SD) differences across the non-gated and the cardiac-gating data (subtracting the SD in the cardiac-gating from the SD in the non-gated group). Note that a higher SD within the mesencephalon (left) and superior cerebellum (right) is seen in the non-gating data at the group level (red to yellow color scheme with small differences encoded in red and large differences encoded in yellow).

3.1.2 Diffusion tensor parameters analysis

At the individual level, more volunteers had a smaller FA value and a bigger MD value in the cardiac-gating group than the non-gating group and the difference range was -0.004 ~ -0.024 in FA and 0.007 ~ 0.026 ($\times 10^{-3}$) in MD (Fig. 5). At the group level, the mean FA value in cardiac-gating group was 0.468 (±0.016) on the left hemisphere and 0.450 (±0.020) on the right hemisphere. In the non-gating group, the mean FA value was 0.473 (±0.018) on the left side and 0.457 (±0.019) on the right hemisphere. After a paired t-test, the statistical P value in the left hemisphere was 0.083 and 0.002 (<0.05) in the right hemisphere. The mean MD value in the cardiac-gating group was 0.822 (±0.035) $\times 10^{-3}$ in the left hemisphere and 0.850 (±0.038) $\times 10^{-3}$ in right hemisphere. In the non-gating group, mean MD value was 0.819 (±0.030) $\times 10^{-3}$ in the left hemisphere and 0.846 (±0.036) $\times 10^{-3}$ in the right hemisphere. Using a paired t-test, the P value in the left hemisphere was 0.422 and 0.298 in the right hemisphere.

A slice analysis showed significantly smaller FA value (P<0.05) at the level of the BS and PLIC with a range of -0.008– -0.016 and a significantly higher MD value (P<0.05) at the level of the PLIC with a range of 0.007–0.018 ($\times 10^{-3}$) (Fig. 5). All the results in Fig.5 were filter and displayed only when there was statistical significance.

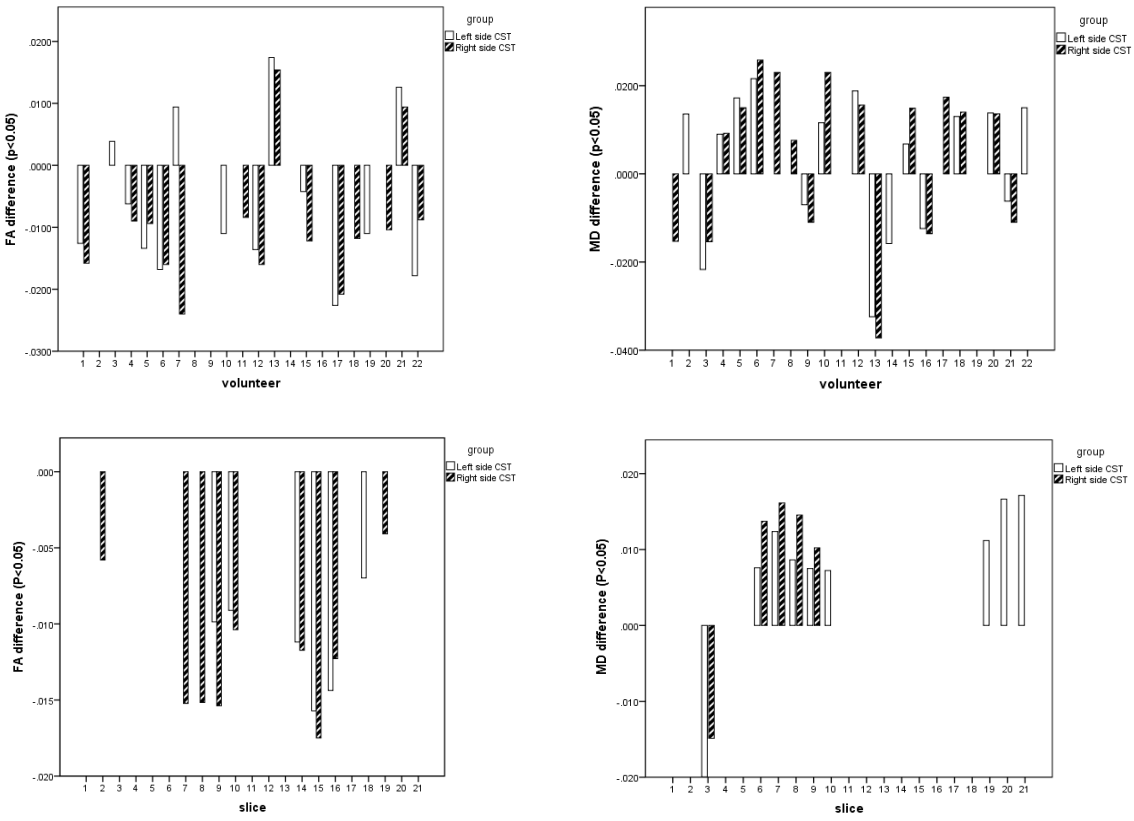

Fig.5: Analysis of the FA and MD within the masked CST. All the results were filtered and displayed only when there was statistical significance (P<0.05). Top: General analysis of the FA and MD within the masked whole CST for each volunteer showing significant FA differences (left) and MD differences (right) between the non-gating and cardiac-gating data. Bottom: Analysis of FA and MD differences within the CST between the non-gating and cardiac-gating data sets within defined sections: brainstem (slices 1–5), posterior limb of internal capsule (slices 6–10), corpus callosum (slices 11–13), cingulum (slices 14–18), and motor cortex (slices 19–21).

3.1.3 TBSS analysis

With TBSS, we analyzed the differences in FA, MD, L1, L2, and L3 values within voxels between the non-gating and cardiac-gating images (Fig. 6). In the region of the CST, including the BS, PLIC and SC, the FA values decreased in all three parts after cardiac-gating. The MD values increased in the BS and PLIC parts. No significant difference was observed in the L1 values. The L2 value increased in the BS and PLIC parts and L3 increased in all the three parts. On comparing the left and right hemispheres, we found that larger clusters of significant differences occurred in the right hemisphere. Table 1 summarizes the changes in FA, MD, L1, L2, and L3 after cardiac-gating. Regarding the slices, a higher FA value and smaller MD, L2, and L3 values were seen in the corpus callosum (CC), especially the genu

and splenium of the CC and the internal capsule of the anterior limb (ALIC) in the cardiac-gating group compared with the non-gating group ($P<0.05$). However, there was an opposite change, with a smaller FA value and larger MD value, in the PLIC in the cardiac-gating group ($P<0.05$).

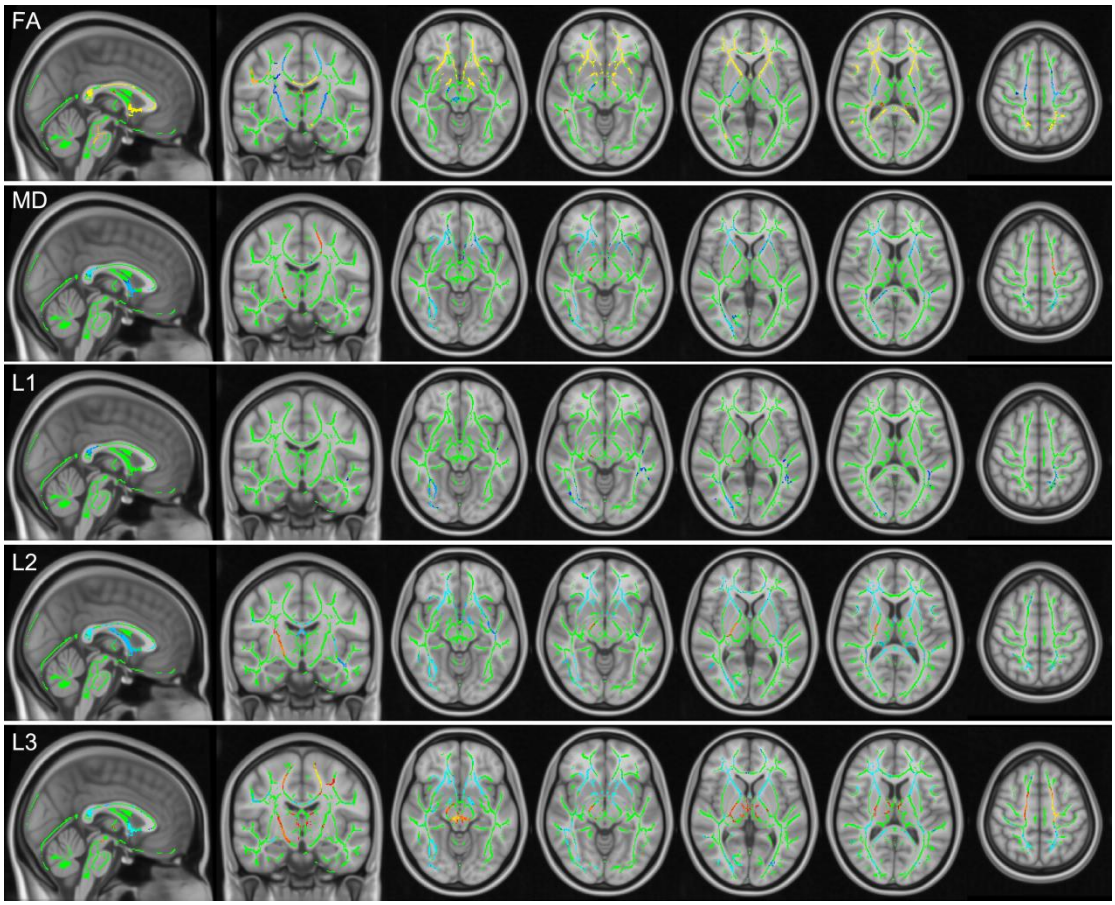

Fig.6: TBSS analysis of the diffusion tensor parameters including the FA, MD, and eigenvalues of L1, L2, and L3. The green line is the skeleton template of the white matter. This line changes from yellow to red when the value is higher in the cardiac-gating group, while the blue color indicates that the value is smaller in the cardiac-gating group.

Table 1: Change in the diffusion tensor parameters after cardiac-gating

Location	FA	MD	L1	L2	L3
BS	—(R)*	+(R)	/	+(R)	+(R)
PLIC	—	+(R)	/	+(R)	+
SC	—	/	/	/	+
Genu CC	+	—	/	—	—
Splenium CC	+	—	—	—	—
ALIC	+	—	/	—	—

*: R indicates a significant difference only in the right hemisphere.

3.1.4 Principal eigenvector analysis

Voxel-wise TBSS analysis of the alteration of the principal eigenvector V1 demonstrated a significant increase in the angle from V1 to the Z-axis in the bilateral BS and PLIC in the cardiac-gating group ($P<0.05$) (Fig.7). Using slice analysis, we found that the angle difference between the non-gating and cardiac-gating group in the BS and PLIC was about 1 ∽ 4 °(Fig. 8).

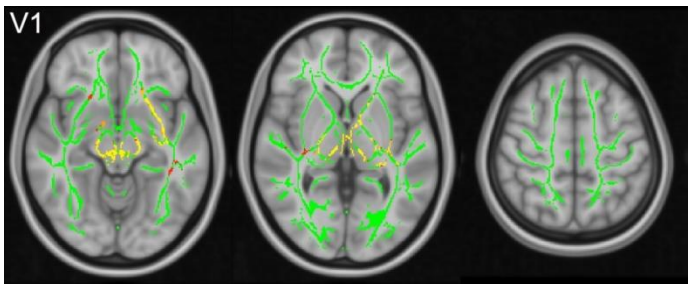

Fig.7: TBSS analysis of the principal eigenvector (V1). The green line is the skeleton template of the white matter. This line changes from yellow to red when the subspace angle of V1 is higher in the cardiac-gating group, while the blue color means that the subspace angle of V1 is smaller in the cardiac-gating group.

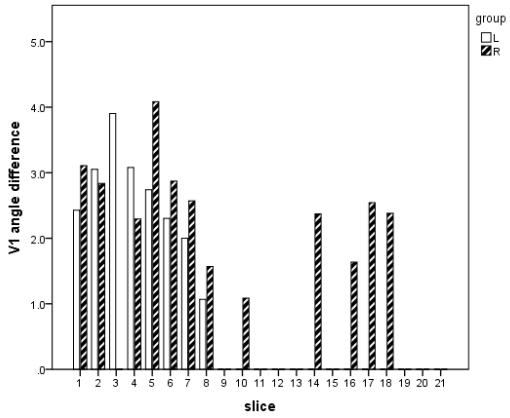

Fig.8: Slice analysis of the principal eigenvector (V1). The difference in the subspace angle V1 was calculated by subtracting the non-gating angle from the cardiac-gating angle (brainstem (slices 1–5), posterior limb of internal capsule (slices 6–10), corpus callosum (slices 11–13), cingulum (slices 14–18), motor cortex (slices 19–21)).

3.1.5 Tractography in the CST

Tractography in the CST in both the non-gating and cardiac-gating group was acquired (Fig. 9). There was no obvious difference between these two groups. The whole CST volume in the

left hemisphere was 13.72±2.38 cm^3 (range from 7.37 cm^3 to 18.83 cm^3) in the non-gating group and 13.84±2.32 cm^3 (range from 8.50 cm^3 to 19.44 cm^3) in the cardiac-gating group (P value=0.551). In the right hemisphere, the whole CST volume was 12.69±2.20cm^3 (range from 7.55 cm^3 to 16.98 cm^3) in the non-gating group and 12.35±2.26 cm^3 (range from 6.37 cm^3 to 17.44 cm^3) in the cardiac-gating group (P value=0.370).

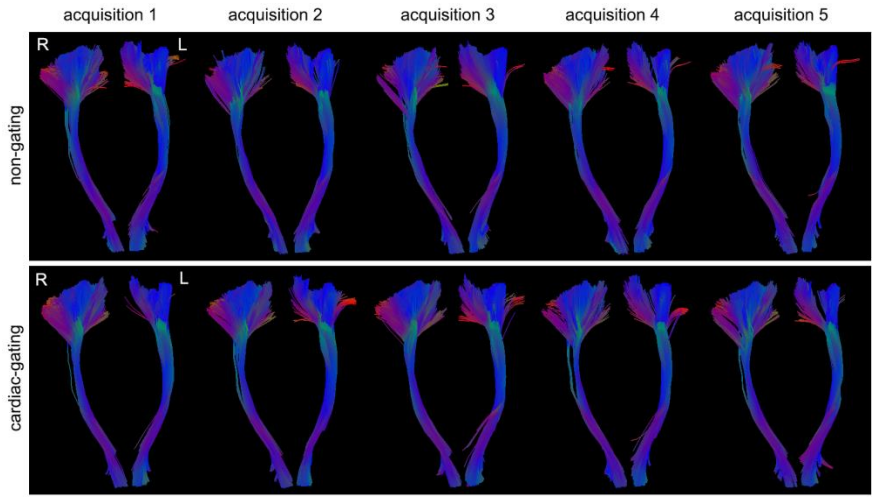

Fig.9: Fiber tractography of the CST in one participant. In the upper row, five CSTs were obtained from five repetitive acquisitions in the non-gating setting, and in the lower row, five CSTs were obtained from the cardiac-gating acquisitions.

3.1.6 Analysis of the tract variability

In the left CST, the JD in the non-gating group was 0.52±0.11 and 0.54±0.07 in the cardiac-gating group (paired t-test, P value=0.41). In the right CST, the JD in the non-gating group was 0.53±0.12 and 0.57±0.10 in the cardiac-gating group (paired t-test, P value= 0.06). Then, we also calculated the JD value in a separate part of CST, including the BS, PLIC and SC. Table 2 displayed the volume and JD value in the whole CST and in three parts of CST. In part of the BS, the JD value in the left hemisphere was 0.53±0.14 (non-gating) vs. 0.54±0.08 (cardiac-gating) (P=0.53), and in the right hemisphere this value was 0.54±0.13 (non-gating) vs. 0.56±0.10 (cardiac-gating) (P=0.53). In part of the PLIC, the JD value was 0.47±0.08 (non-gating) vs. 0.48±0.08 (cardiac-gating) (P=0.44) in the left hemisphere, and in the right hemisphere this value was 0.48±0.11 (non-gating) vs. 0.51±0.09 (cardiac-gating) (P=0.19). In part of the SC, the JD value in the left hemisphere was 0.57±0.16 (non-gating) vs.

0.56±0.09 (cardiac-gating) (P=0.77), and 0.53±0.13 (non-gating) vs. 0.60±0.12 (cardiac-gating) (P=0.02) in the right hemisphere.

Table 2: Tract volume and Jaccard distance (JD) along the CST and its subdivisions (BS, PLIC, and SC) between non-gating (NG) and cardiac-gating (G) group

	Hemisphere	Group	Tract volume (mean±SD)	P value	JD (mean±SD)	P value
CST	L	NG	13.72±2.38	0.55	0.52±0.11	0.41
		G	13.84±2.32		0.54±0.07	
	R	NG	12.69±2.20	0.37	0.53±0.12	0.06
		G	12.35±2.26		0.57±0.10	
BS	L	NG	2.51±0.49	0.48	0.53±0.14	0.53
		G	2.45±0.60		0.54±0.08	
	R	NG	2.45±0.46	0.13	0.54±0.13	0.53
		G	2.32±0.48		0.56±0.10	
PLIC	L	NG	3.23±0.70	0.06	0.47±0.08	0.44
		G	3.12±0.61		0.48±0.08	
	R	NG	3.01±0.59	0.15	0.48±0.11	0.19
		G	2.84±0.46		0.51±0.09	
SC	L	NG	7.96±1.67	0.18	0.57±0.16	0.77
		G	8.28±1.74		0.56±0.09	
	R	NG	7.61±1.59	0.26	0.53±0.13	0.02
		G	7.31±1.61		0.60±0.12	

3.2 Results of part 2: POAS and DWI

3.2.1 Inspection of the DWI images and estimation of the SNR

The POAS-processed and the averaged DWI data from the same gradient direction were compared (Fig.10). In the B0 images, there was no obvious difference among these three groups. However, in the diffusion weighted images with a b value of 1000 s/mm^2, the difference was easy to determine. Images from the original data presented more noise in the

brain parenchyma and presented an unclear boundary between the grey matter and the white matter. After image averaging, the image quality increased. The noise in the brain decreased and the contrast among the different structures improved in the averaged image. In the POAS-processed DWI, there was less noise than the averaged DWI in the brain parenchyma and differentiation between the grey matter and the white matter was still possible. No obvious blurring occurred in the POAS-processed DWI and there was no decrease in image intensity as well.

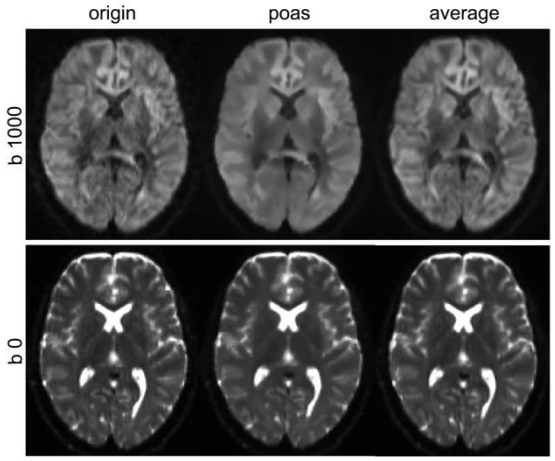

Fig.10: DWIs from the original, POAS-processed, and averaged datasets. The upper row shows the diffusion weighted images with b=1000 s/mm2, the lower row shows the non-diffusion weighted images with b=0 s/mm2.

Then, the SNR was quantitatively estimated to compare the image quality among the three groups. After calculation with the same ROIs, the SNR in the POAS-processed DWIs was 218.27±78.09, which was much higher than that both of the averaged DWIs having an SNR value of 178.70±64.59 and in the original DWIs of 133.33±32.60. The randomized block design of the ANOVA test indicated a significant difference among these three groups ($P<0.001$). Then, a pairwise comparison with Tukey's HSD test also indicated a significant difference between the original and POAS-processed data, the original and averaged data, and the POAS-processed and the averaged data (P value for the three comparisons: <0.001, <0.001, <0.001 respectively).

3.2.2 TBSS analysis of the FA and MD values

A whole brain TBSS analysis was conducted to estimate the differences in the FA values

among the three groups. The results of the TBSS analysis displayed a statistical significance ($P<0.05$) (Fig.11). In contrast, analysis of the original and the POAS-processed data indicated that after denoising with POAS, the FA value decreased significantly in the whole brain. Meanwhile, after averaging, the FA value also decreased significantly compared with the FA value from the original DWI. Finally, we performed a comparison of the FA value between the POAS-processed datasets and the averaged datasets and found that the FA value from the POAS-processed DWI was still significantly lower than the FA value from the averaged DWI. In the TBSS analysis of the MD, comparison between the original and POAS-processed datasets revealed that some parts of the white matter had an increased MD value in the POAS-processed datasets compared to the original datasets, for example the corpus callosum, while some other regions showed a lower MD value in the POAS-processed datasets or no difference between these two groups. The same findings were noted in the comparisons between the MD values from the averaged and POAS-processed datasets. There was no significant difference between the MD values from the original and averaged datasets.

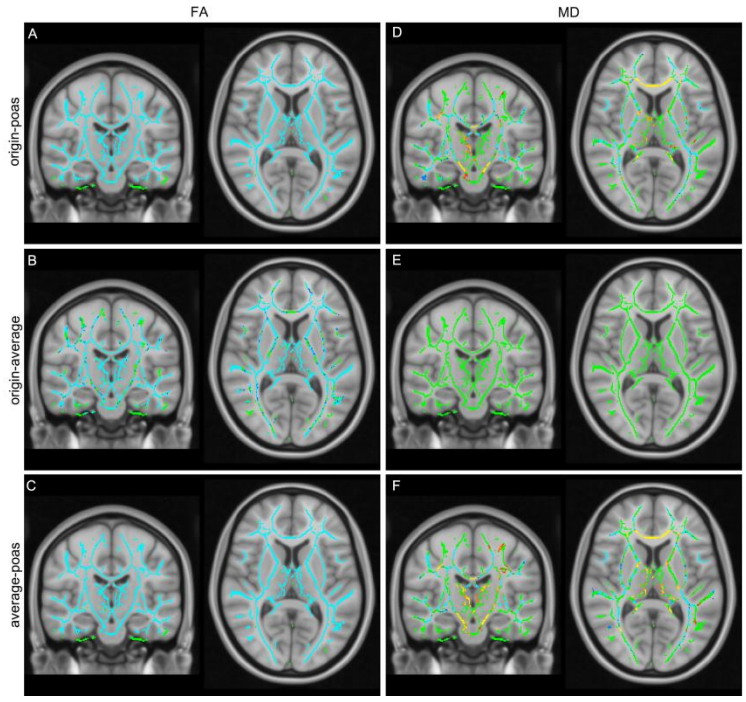

Fig.11: TBSS analysis of the whole brain FA and MD values. The green line is the background of a standard mean FA skeleton. A: the blue color of the skeleton indicates a lower FA value in the POAS compared to the origin group; B: the blue color of the skeleton indicates a lower FA value in the average group compared to the original group; C: the blue color of the skeleton indicates a lower FA

value in the POAS group compared to the average group; D: the blue color of the skeleton indicates a lower MD value in the POAS group compared to the original group, and the yellow to red color indicates a higher MD value in the POAS group compared to the original group, for example in the corpus callosum; E: there was no significant difference in the MD value between the original and average group; F: the blue color of the skeleton indicates a lower MD value in the POAS group compared to the original group, and the yellow to red color indicates a higher MD value in the POAS group compared to the original group, for example in the corpus callosum.

3.2.3 Variability assessment of DWI and FA

A variability analysis was conducted between the original and POAS-processed data with the CV maps and the difference-CV map which was obtained by subtracting the CV-POAS map from the CV-origin map. The mean CV in the DWI signal intensity was 0.072±0.034 (original data) and 0.042±0.031 (POAS processed data). The mean CV in FA was 0.156±0.072 (original data) and 0.153±0.079 (POAS processed data). After statistical comparison, there was a significant difference in the CV value between the original and the POAS processed data (DWI signal intensity: $P<0.001$; FA: $p=0.006$). To further compare the variability in the whole brain, the CV maps and the difference CV map was constructed (Fig. 12). In both of the DWI and FA maps, more prominent difference between the original and POAS processed data was located in the white matter especially in the thalamus, this indicating that the original datasets had a higher variation in these regions than the POAS-processed datasets. According to the histogram graph of the difference-CV map, a shift towards positive value was observed from the distribution and the area under curve (AUC) was also positive, thus proving there was a higher variation in DWI and FA in the original datasets compared to the POAS-processed datasets in the whole brain.

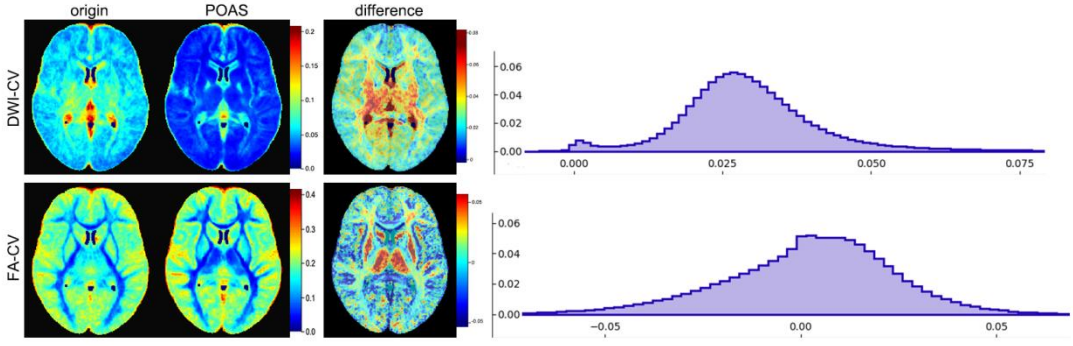

Fig.12: CV maps from the original and POAS processed data, the difference-CV map and the relative

histogram graph in DWI intensity and FA values. The difference-CV map was calculated by subtracting the CV-POAS map from the CV-origin map. This color map of the difference-CV map was obtained by averaging the difference-CV maps for each volunteer.

3.2.4 Tractography of the CST

After automated fiber tracking, the CSTs in the three groups were acquired (Fig.13). Slight differences were observed in the region above the internal capsule, especially in the motor cortex. CSTs with wider extended streamlines were displayed in the motor cortex in the POAS-processed datasets compared to both the original and averaged datasets. A more balanced and smoother distribution of the fiber tracts was seen in the CST-POAS compared to the CST-origin. Even in the averaged data with deterministic algorithms (CST-average), the streamlines were less uniform than the CST-POAS. After we set the CST reconstructed from the averaged data with a CSD algorithm as the standard reference (CST-reference), we found that depending on the shape and location of the fiber tracts, the CST-POAS was more like the CST-reference.

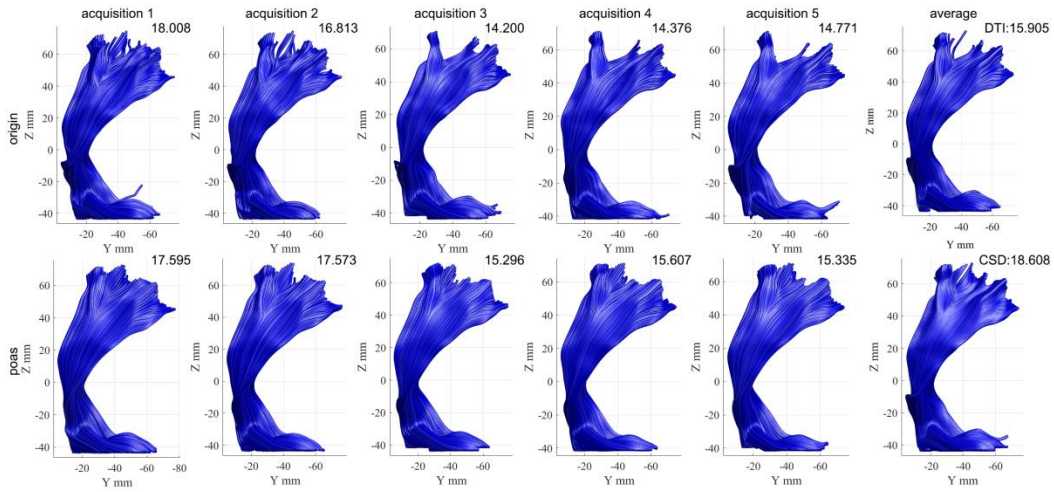

Fig.13: Tractography of the CST in volunteer 1 including 5 CST-origins, 5 CST-POASs, 1CST-average with a deterministic FACT algorithm, and 1 CST-reference with a CSD algorithm (the number in the upper right part of the CST is the tract volume(ml)).

3.2.5 Tract profile of CST

The tract profile of the CST was analyzed including the CST fiber volume, FA value, MD value and fiber density (Table 3). The volume of the CST-reference was 14.01±3.30 ml in the left hemisphere and 17.46±4.11 ml in the right hemisphere. In the left hemisphere, the CST

volumes were 11.32±2.85 ml (CST-origin) vs. 11.82±2.64 ml (CST-POAS) vs. 11.47±2.93 ml (CST-average) (P=0.030). In the right hemisphere, the CST volumes were 14.37±3.37 ml (CST-origin) vs. 14.88±3.22 ml (CST-POAS) vs. 14.63±3.49 (CST-average) (P=0.018). Then using Tukey's HSD test, we obtained a P value of 0.027 (CST-origin vs. CST-POAS), 0.150 (CST-POAS vs. CST-average), and 0.714 (CST-origin vs. CST-average) in the left hemisphere, and 0.014 (CST-origin vs. CST-POAS), 0.323 (CST-POAS vs. CST-average), and 0.297 (CST-origin vs. CST-average) in the right hemisphere.

Table 3: Tract profile of the CST including fiber volume, FA value, MD value and fiber density

Type	Side	Origin	POAS	Average	P value* (origin vs. POAS vs. average)	P value# (origin vs. POAS)	P value# (origin vs. average)	P value# (POAS vs. average)
CST volume	L	11.32±2.85	11.82±2.64	11.47±2.93	0.030	0.027	0.714	0.150
	R	14.37±3.37	14.88±3.22	14.63±3.49	0.018	0.014	0.297	0.323
FA value	L	0.616±0.024	0.568±0.027	0.613±0.025	<0.001	<0.001	0.469	<0.001
	R	0.593±0.026	0.547±0.030	0.588±0.027	<0.001	<0.001	0.092	<0.001
MD value	L	0.723±0.020	0.714±0.019	0.722±0.020	<0.001	<0.001	0.506	<0.001
	R	0.729±0.020	0.720±0.020	0.727±0.020	<0.001	<0.001	0.150	<0.001
Fiber density	L	65.50±6.48	64.30±6.84	65.59±7.80	0.151	0.234	0.991	0.188
	R	65.91±6.13	62.29±5.38	66.36±6.65	<0.001	<0.001	0.720	<0.001

*: with a randomized block design ANOVA test; #: with Tukey's HSD test for pairwise analysis

&: origin: original datasets; POAS: POAS-processed datasets; average: averaged datasets

Then, we obtained the FA value of the CST in each group. In the left hemisphere, the FA value of CST was 0.616±0.024 (original datasets) vs. 0.568±0.027 (POAS-processed datasets) vs. 0.613±0.025 (averaged datasets) (P<0.001), and in the right hemisphere, the FA value was 0.593±0.026 (original datasets) vs. 0.547±0.030 (POAS-processed datasets) vs. 0.588±0.027 (averaged datasets) (P<0.001). Then, a Tukey's HSD test was conducted for the following pairwise comparisons; original vs. POAS-processed datasets, POAS-processed vs. averaged datasets, which indicated a significant statistical difference (all P values <0.001 in both

hemisphere). However, the FA value between the original and averaged datasets did not obtain a significant difference (P value: 0.469 in left, 0.092 in right). Detailed MD values in each group were seen in the table and there was also a statistical difference among these three groups. Pairwise tests indicated a significantly higher MD value in the original datasets compared to the POAS-processed datasets and a significantly higher MD value in the averaged datasets compared to the POAS-processed datasets. There was no significant difference between the original and average group in terms of MD values.

For fiber density, a statistical difference was observed only in the right hemisphere of the CST ($P<0.001$) but not in the left hemisphere ($P=0.151$) among the three groups. The fiber densities in the left hemisphere were 65.50 ± 6.48 (CST-origin) vs. 64.30 ± 6.84 (CST-POAS) vs. 65.59 ± 7.80 (CST-average), and in the right hemisphere they were 65.91 ± 6.13 (CST-origin) vs. 62.29 ± 5.38 (CST-POAS) vs. 66.36 ± 6.65 (CST-average). The lowest fiber density was in the CST-POAS. We also found that the fiber density in the CST-reference was rather large with 464.20 ± 65.65 in the left side and 500.88 ± 45.91 in the right side. A pairwise comparison of fiber density showed no difference between any of the groups in the left side of the CST but a significant difference was noted in the right hemisphere in the following pairwise comparisons; CST-origin vs. CST-POAS and CST-POAS vs. CST-average ($P<0.001$ and $P<0.001$ respectively).

3.2.6 Reproducibility and similarity of the analysis of the CST

Reproducibility analyses among the five CST-origins or five CST-POASs were performed separately via calculation of the Jaccard index (JI) (Table 4). We got the JI-origin of 0.313 ± 0.048 and JI-POAS of 0.408 ± 0.071 in the left hemisphere ($P<0.001$), and in the right hemisphere the JI-origin was 0.372 ± 0.059 and the JI-POAS was 0.457 ± 0.055 ($P<0.001$).

The similarity between the CST-origins and CST-POASs was estimated also with the Jaccard index. In the left hemisphere, the JI between the CST-origins and CST-POASs was 0.625 ± 0.045, and in the right hemisphere JI was 0.657 ± 0.051. We also calculated the similarity between the CST-origin and CST-reference and between CST-POAS and

CST-reference separately. The JI between CST-origin and CST-reference was 0.641±0.057 in the left hemisphere and 0.687±0.053 in the right hemisphere. The JI between CST-POAS and CST-reference was 0.599±0.054 in left and 0.643±0.053 in the right hemisphere. A comparison was conducted with a Wilcoxon signed-rank test and a significant difference was noted on both sides (P value: <0.001 in left, <0.001 in right).

Table 4: Results of the reproducibility and similarity analyses evaluated with the Jaccard index

Type	Side	Group	Jaccard index	P value
Reproducibility	L	origin	0.313±0.048	<0.001#
		POAS	0.408±0.071	
	R	origin	0.372±0.059	<0.001#
		POAS	0.457±0.055	
Similarity	L	origin-POAS	0.625±0.045	<0.001*
		origin-average	0.654±0.058	
		POAS-average	0.596±0.055	
	R	origin-POAS	0.657±0.051	<0.001*
		origin-average	0.701±0.052	
		POAS-average	0.643±0.052	
Similarity	L	origin-reference	0.641±0.057	<0.001&
		POAS-reference	0.599±0.054	
	R	origin-reference	0.687±0.053	<0.001&
		POAS-reference	0.643±0.053	

#: with a paired t test; *: with a randomized block design ANOVA test

&: with a Wilcoxon signed-rank test

origin: original datasets; POAS: POAS-processed datasets; average: averaged datasets

4. Discussion

4.1 Discussion of Part 1: cardiac-gating and DWI

Since DWI is being more and more widely applied, precise DWI acquisition is necessary. Pulsatile motion, which is characterized by a greater movement than Brownian motion, has been reported to result in motion artifacts in DWI, calculation bias of the diffusion tensor parameters and error in tractography (*Habib et al. 2009,Habib et al. 2010,Pierpaoli et al. 2003*). However, debate still exists because in some reports some researchers were unable to detect any noticeable motion artifacts (*Nagy et al. 2008*). Therefore, entirely different results were obtained. Our study aimed to identify if pulsatile motion was able to influence DWI and if cardiac-gating could fix the bias produced by pulsatile motion. We investigated the effects of pulsatile motion on DWI, focusing especially on the CST region. We detected the motion artifacts, bias of the diffusion tensor parameters and fiber tractography in the CST and measured the ability of cardiac-gating in reducing the pulsatile motion effect.

First, we observed the image artifacts in non-gating and cardiac-gating DWIs. It was previously believed that pulsatile motion could produce motion artifacts with signal attenuation or signal loss, and cardiac-gating could help to eliminate or avoid these artifacts. In our study, obvious artifacts occurred in non-gating DWIs in the mesencephalon and cerebellum, and not only in volume 24 but also in volume 17. In cardiac-gating DWIs, there were no obvious pulsatile motion artifacts. At the same time, after image averaging, no obvious artifacts were observed in the non-gating or in the cardiac-gating groups. Therefore, we proved that in our study setting, cardiac-gating could help to eliminate the pulsatile motion artifacts in DWIs.

Volume 24 had the smallest subspace angle from gradient direction to Z axis, was characterized by higher occurrence rate of artifacts (11.81%) than in volume 17 (4.55%) which had a subspace angle closer to 90 °. The occurrence ratio of pulsatile motion artifacts in our study was consistent with the range in previous reports of about 6%~20% (*Nunes et al. 2005,Skare, Andersson 2001*). Previous researches demonstrated obvious motion artifacts in

the brain stem, cerebellum, thalamus, and CC (*Chung et al. 2010,Greitz et al. 1992*). However, the artifacts reported in previous articles were much more severe and had more signal attenuation than the images used in our study, and almost all the images in previous articles with prominent artifacts came from the gradient direction along the Z axis (*Chung et al. 2010,Pierpaoli et al. 2003,Skare, Andersson 2001*). Normally, after setting up the AC-PC line as the axial level, the brain stem is usually located along the Z axis. Therefore, more obvious artifacts are present in the brain stem when the gradient direction is along Z axis (*Chung et al. 2010,Habib et al. 2010,Skare, Andersson 2001*). In DWI acquisition, at least six non-collinear gradient directions are necessary for fiber tracking and it is rare that one of the gradient directions is completely along Z axis. Almost all of the gradient directions have a deviation from the Z axis. However, volume 24 had the smallest subspace angle of $18.77° \pm 5.42°$ on average, which was the smallest subspace angle from the gradient direction to the Z axis. Therefore, this deviation of the subspace angle might weaken the effect of the pulsatile motion on DWI images. Moreover, we also found that in volume 17, which had a subspace angle closer to 90°, there was a significantly lower occurrence ratio of pulsatile motion artifacts. Until now only one research demonstrated the DWI signal artifacts from 16 gradient directions, and this was from a case involving a 1-month-old infant. In this study pulsatile motion artifacts also occurred in the brain stem and cerebellum and were similar to the artifacts presented in our study, which were not as severe as the artifacts presented in other reports characterized by more signal attenuation (*Kozák et al. 2013*).

What was unique in our study was that we performed repetitive acquisitions both in the non-gating and the cardiac-gating group and evaluated the image variation between these two groups. We obtained an SD map and found prominent signal variations with a greater SD in the mesencephalon and cerebellum in non-gating DWIs, coincident with the areas of motion artifacts in DWIs.

After showing that cardiac-gating could eliminate the occurrence of DWIs artifacts and image variation, we wanted to determine if these changes were helpful in improving the accuracy of the diffusion tensor parameters. Only a few articles with a few volunteers reported changes in

FA, MD or ADC values produced by pulsatile motion. These studies detected changes in the whole brain, CC, thalamus or a slice of the midbrain (*Habib et al. 2008,Nakamura et al. 2009*), but were not focused on a specific white matter fiber bundle and did not explore any changes in the eigenvectors. Obviously, the changes in the diffusion tensor parameters in the fiber bundles are related to fiber tractography. Therefore, in this study we aimed at studying the diffusion tensor parameters in the CST. Group analysis demonstrated that pulsatile motion resulted in an over-estimation of the FA value and an under-estimation of the MD value, and cardiac-gating decreased the FA value and increased the MD value. TBSS analysis showed that over-estimation of the FA value occurred in the BS, PLIC and SC, while under-estimation of the MD values occurred in the BS and PLIC. This bias in FA and MD was attributable mainly to L2 and L3, not to L1. The CST is a highly anisotropic tract, which means that the L1 value in the CST should be much larger than L2 and L3 value. Therefore, although pulsatile motion is larger than Brownian motion, it is unable to easily produce a significant bias in L1.

From the TBSS analysis, we also observed that in some of the diffusion tensor parameters such as FA, MD, L2, L3 in the right hemisphere, there were bigger areas and more slices with a significant difference between non-gating and cardiac-gating datasets. In our study, the FA value in the left hemisphere was larger than in the right hemisphere, in agreement with previous reports about CST asymmetry (*Vos et al. 2016*). Therefore, a higher anisotropy in the left CST made it more resistant to changes due to pulsatile motion. This finding explains why the diffusion tensor parameters had more areas in the right hemisphere with a significant difference between non-gating and cardiac-gating. In locations other than the CST, like the CC and ALIC, opposite changes were observed. The CC, ALIC and PLIC all belong to highly anisotropic tracts. However, the direction of the tract pathway is quite different with ALIC running in an anterior-posterior direction, the CC running in a left-right direction and the PLIC running in a superior-interior direction. Although pulsatile motion is very complicated, the brain would move in a (head-feet) direction, as if it needed to run away from the skull because of the increased cranial pressure during the systolic period (*Greitz et al. 1992*).

However, the motion direction may be entirely different in each part of the brain. Therefore, it is easy to understand that pulsatile motion might have different effects on different regions with different fiber bundle pathways.

The TBSS analysis as well as the slice analysis of the principal eigenvector (V1) showed that pulsatile motion made the direction of V1 a little closer to the Z axis, which was about 1 ° ~ 4 °. Previous reports also analyzing V1, observed this change in angle of V1 in the cerebellum, which had an angle difference of 27 ° (*Kozák et al. 2013*). A previous report detected an angle difference of less than 5 ° in the CC and transverse fibers in the brain stem (*Walker et al. 2011*). In this study, based on the TBSS analysis and on the slice analysis, we investigated the angle difference of V1 in the CST between non-gating and cardiac-gating groups and found obvious angle differences in the BS and PLIC. Pulsatile motion induced noticeable motion artifacts in the BS, but this was unable to influence the principal eigenvalue but resulted in a change in the direction of the principal eigenvector.

Fiber tractography is an important aspect of surgery guiding. DWI with at least six gradient directions is the basis for fiber tracking. More gradient directions, also meaning a higher angular resolution, can decrease tractography variation and improve the accuracy of localization (*Tournier et al. 2011,Vos et al. 2016*). DWI spatial resolution helps to distinguish neighboring structures within the brain (*McNab et al. 2009*). Noise decreases the spatial resolution which affects spatial accuracy in tractography. The angular resolution which is related to the amount of gradient direction plays a more critical role than spatial resolution in tractography, and decreases the variation of CST tractography (*Vos et al. 2016*). Previous studies reporting the effect of pulsatile motion on the diffusion tensor parameters, utilized 6 or 15 diffusion gradient directions. The research, which focused on the effect of pulsatile motion on tractography, used a probabilistic algorithm and had six gradient directions (*Habib et al. 2008,Jones, Pierpaoli 2005,Nakamura et al. 2009*). In our study, pulsatile motion produced image artifacts, bias of the diffusion tensor parameters and deviation of the V1 direction, but the CST volume did not present significant differences between the non-gating and the cardiac-gating group in the whole CST and in three parts of the CST. We detected the tract

variation with JD, and after the comparison we observed that there was no significant difference in the variation of the CST from the repetitive acquisitions. This finding may have been due to the utilization of 30 gradient directions, therefore the variation in either group decreased and the difference was diluted between non-gating and cardiac-gating data. However, here we used a deterministic algorithm instead of the probabilistic algorithm used in a previous article. The authors in that study reported that cardiac-gating could help to reduce false-negatives in tractography (*Jones, Pierpaoli 2005*). However, in our study using a deterministic algorithm, cardiac-gating did not improve the volume of the CST or the accuracy of occupancy.

The debate on the influence of pulsatile motion and the necessity of cardiac-gating existed because some studies reported that the effect of pulsatile motion in the brain was not pronounced and that cardiac-gating did not result in prominent improvements. Some alternative methods were reported which could have a similar effect to cardiac gating, including multi-scanning and image averaging, applying Zero-Padding reconstruction approaches or a full Fourier acquisition approach. These methods were either insensitive to motion, or used a filtering algorithm to remove motion noise (*Chang et al. 2005,Chang et al. 2012,Chung et al. 2010,Nunes et al. 2005,Parker et al. 2000,Robson, Porter 2005*). Among these approaches, image averaging seemed to be an easy way to achieve the desired outcomes. In this study, we also observed that after image averaging, there was almost no signal difference in DWI between the non-gating and the cardiac-gating group. Although averaging diluted the random occurrence of motion artifacts, it did not eliminate the difference in FA, MD and V1 between the non-gating and cardiac-gating datasets. Differences in the diffusion tensor parameters in the general analysis of the whole CST disappeared after averaging, but in the analysis of the voxel CST these differences persisted. Therefore, in this study we found that averaging did not completely substitute cardiac-gating. Additionally, in our method, the acquisition time with cardiac-gating was no more than two times the non-gating time. Therefore, cardiac-gating also had the benefit of time saving compared with averaging.

There was a possible drawback coming from SNR in our study. We did not know if SNR

influenced the difference in the diffusion tensor parameters between the non-gating and cardiac-gating datasets. With the cardiac-gating approach, the variable TR produced a different SNR compared with the non-gating approach. It was also reported that the SNR could influence the FA and MD values. When the SNR decreased, there was an upward bias in the FA and no bias in MD (*Farrell et al. 2007*). Therefore, in further research more attention should be paid to the effect of SNR caused by pulsatile motion.

There are four mechanisms that can lead to pulsatile motion, including arterial pulse, venous expansion, CSF flow and capillary expansion. Phase-velocity measurements have shown that the highest velocities are present in the inferior and medial areas of the brain and decrease towards the periphery (*Greitz et al. 1992*). The motion caused by microvascular or capillary expansion normally occurs in the parenchyma, which is also called intravoxel incoherent motion (IVIM) (*Federau et al. 2013,Kang et al. 2017,Le Bihan et al. 1986,Le Bihan et al. 1988*). This kind of motion has been described early and represents perfusion and diffusion at the same time. It can be observed only when the b-value is lower i.e. no more than 1000 s/mm. In this study, we had a b-value of 1000 s/mm. Therefore, IVIM did not contribute to the motion effect. Arterial pulse, venous expansion and CSF flow occur mostly in the cranium base and in the medial part of the brain. The motion artifacts we observed in this study belonged to these regions. Normally, pulsatile motion does not affect T1 or T2, because T1 and T2 occur with faster scanning and are not sensitive to the minimal movement associated with DWI. However, in pathological situations like normal pressure hydrocephalus and Chiari I malformations (*Kan et al. 2015,Radmanesh et al. 2015*), obvious brain displacements of about 1~4 mm have been observed. Therefore, more studies are needed to identify which diseases affect brain dynamics and the effects of pulsatile motion and function of cardiac-gating in pathological cases.

4.2 Discussion of Part 2: POAS and DWI

In this part of the study, we analyzed the contribution of POAS in the diffusion tensor properties and the tractography of the CST. POAS is a kind of denoising approach with good edge-preserving properties for fine and anisotropic structures. Based on the algorithm of

POAS, blurring of the inherent structures is avoided and any discontinuities are avoided (*Becker et al. 2012,Becker et al. 2014*). In our study we also found that DWI processed with POAS had a dramatically decreased background noise compared with the original datasets and the structural boundaries were clear and did not present obvious blurring between the grey and white matter. When comparing with the averaged datasets, the POAS-processed DWI had less noise and maintained a distinct differentiation. Then, SNR evaluation resulted in a quantitative comparison of the image quality. After statistical calculation, although the SNR in the averaged DWIs was obviously increased compared with the original DWIs, the SNR in the POAS-processed DWIs was the greater than both the original and averaged datasets with statistical significance. Consequently, for POAS, the gain in SNR was quite substantial and this benefit came from the fact that this algorithm considered the geometric properties of the measurement space. When considering the conflict between spatial resolution and SNR, by improving SNR, POAS may be used to compensate the shortages inherently produced by a higher spatial resolution.

POAS could reduce noise and enhance SNR. Typically, noise in DWI introduces systematically biased measurement, such as in the diffusion metrics, FA and MD (*Basser, Pajevic 2000,Pierpaoli, Basser 1996*). Although many studies displayed different kinds of denoising algorithms, fewer articles investigated the influence of these algorithms on the accuracy of the diffusion metrics. In order to determine if the FA and MD values changed after denoising with POAS, TBSS analysis of the whole scale among the three datasets, original, POAS-processed and averaged datasets, was performed in our study. From the results, the FA value in the averaged datasets decreased significantly in the whole brain. Because averaging is a common and well-known method to improve SNR, and when setting up the average as the reference, the FA value in the original datasets was over-estimated. This was consistent with previous reports. In previous reports the increased SNR indeed was accompanied with a decreased FA value which was in agreement with our results, while the lower SNR resulted in the overestimation of the FA value (*Anderson 2001,Farrell et al. 2007,Jones, Basser 2004,Walker et al. 2009*). Then, comparing between the averaged and

POAS-processed datasets, the FA value from POAS-processed datasets was even less than the averaged datasets and also less than the FA value from the original datasets. This might be relative with the considerable improvement in the SNR in the POAS-processed datasets. Maybe there were same reasons to explain that the SNR was the highest and the FA value was the smallest in POAS-processed datasets among these three groups. However, for the FA value from the POAS-processed datasets and the averaged datasets, determining which one was closer to the real FA value was difficult in this study. Although other denoising methods, conducted on simulated data, are similar to POAS and have been proven to make FA approach its real value, from this study it was hard to identify if POAS could make the FA value more accurate compared to the averaging method (*Manjón et al. 2013*). However, it was clear that POAS could produce a lower variation in the FA value. After we obtained the CV-difference map in the DWI signal intensity and the FA value, a lower CV value was observed in the POAS-processed datasets compared with the original datasets which meant that less variability occurred after POAS denoising. This could also be explained by the less noise in DWI and higher SNR in the POAS-processed datasets.

As we knew, less variation of the FA value is associated with a reliable white matter tractography. We also analyzed the tractography in the CST. For neurosurgical operations, to avoid damage of the CST, an accurate and reliable tractography of the CST is necessary (*Nimsky et al. 2005a, b,Nimsky et al. 2006*). Therefore, we analyzed the CST tractography and the tract profile of the CST including the fiber volume, fiber density, FA and MD values. Although the FA value of the CST-POAS was the smallest among the CST-origin, CST-POAS and CST-average, the fiber volume was not. On the contrary, the fiber volume of the CST-POAS was larger than the CST-origin and CST-average. We found that after the image enhancement by averaging, the CST fiber volume did not increase significantly compared with the CST-origin. However, after denoising with POAS, the CST volume was significantly larger than the CST-origin and there was no statistical difference between the volume of the CST-POAS and CST-average.

Given the tract pathway, the reconstructed CST-POAS was smoother and was characterized

by an accurate anatomic location than the CST-origin and CST-average and appeared similar to the standard reference reconstructed with the CSD algorithm with the average data. The CSD was based on a tensor free model and was an approach to characterize the intra-voxel diffusion behavior (*Tournier et al. 2007,Tournier et al. 2008*). The CSD is able to reconstruct more complex tract architectures than the diffusion single tensor model especially in pathological cases (*Auriat et al. 2015*). Therefore after the comparison, we knew that the CST-POAS could well describe the anatomic structure and location of the CST. We also calculated the reproducibility of these five CST-origins and five CST-POASs separately with Jaccard index (JI). The JI-POAS was significantly higher than JI-origin which meant that CST-POASs had a higher reproducibility and stability than CST-origins. We knew that good reproducibility of the fiber tracts were also one of the aim of a higher angular resolution (*Lenglet et al. 2009,Zhan et al. 2010*). Taking HARDI (high angular resolution diffusion imaging) for example, by adding more diffusion gradients and increasing the b value, the reconstructed fiber tracts could better present the crossing and intermixing of white matter and obtain a more stable tractography, which are both limitations of the normal diffusion single tensor model (*Tuch 1999,Tuch et al. 2002,Zhan et al. 2013*). So in this study, we found that after denoising with POAS, the reconstructed CST could have more stable and reproducible fiber tracts than the CST from the original data and even the averaged data. So POAS could compensate for a high angular resolution to some degree which would produce more stable and accurate fiber tractography.

After comparing the appearance of CST with the CSD method, we also analyzed the quantitative similarity in CST-origin vs. CST-reference and CST-POAS vs. CST-reference respectively. The JI was applied and the JI in CST-origin vs. CST-reference was significantly larger than the JI in CST-POAS vs. CST-reference. Although we also calculated the similarity between CST-origin and CST-POAS and obtained a high similarity value of over 0.6 (0.625 ± 0.045 in left hemisphere and 0.657 ± 0.051 in the right hemisphere), the difference in JI between CST-origin vs. CST-reference and CST-POAS vs. CST-reference was in their meaning. The FA comparison indicated a decreased FA value in the POAS-processed datasets

not only in the whole brain, but also in the specific tracts of the CST. Why did the volume of CST-POAS not decrease when the FA decreased but the JI in CST-POAS vs. CST-reference decreased compared with the original datasets? This finding may be because the CST is inherently a kind of white matter tract with higher fiber integrity. So the fiber volume which represents the spatial occupation of voxels was not affected easily with decrease but on the contrary it increased a little. However, a lower FA may cause a lower fiber density (*Roberts et al. 2005*). After we calculated the fiber density in this study, the lowest value was actually in CST-POAS especially in the right hemisphere with a statistical significance. The lower FA value in the CST-POAS group was related to a lower fiber density. The lower fiber density in CST-POAS may have contributed to the lower similarity between CST-POAS and CST-reference.

Except for POAS, many other denoising approaches have helped to improve image quality, such as Gaussian filtering (*Westin et al. 1999*), wavelet transformation (*Wirestam et al. 2006*), non-linear anisotropic diffusion filter (*Weickert 1998*), the propagation-Separation approach (*Polzehl, Spokoiny 2006*), nonlocal means (*Wiest-Daessl é et al. 2008*) and so on. The POAS was also reported with comparable effect of denoising with other denoising approaches (*Becker et al. 2012,Becker et al. 2014*). POAS produced obvious improvement in SNR and at the same time avoided edge-blurring which is essential for clinical diagnosis. Averaging is a conventional method used to increase SNR by averaging several repetitions of the signal (*Farrell et al. 2007*). It suppresses the effects of random variations or random artifacts and has also been reported to reduce physiological artifacts, like respiratory motion (*Holmes et al. 1998*). However, averaging requires a longer acquisition time which hinders its application in clinical cases. Meanwhile, compared with averaging, POAS improved SNR to a greater extent and produced better fiber tractography results with a comparable fiber volume. Although processing with POAS also took a long time on our PC, the consuming time occurred only in the post processing phase and the MRI scanning for patients was not affected by POAS. Also, a better equipped PC could drastically decrease the processing time and make POAS readily acceptable in a clinical setting.

In the past decades the development of diffusion tensor imaging (DTI) made it more feasible for a broader range of clinical and neuroscience applications. However, DTI cannot present crossing fibers which has always a limitation of its uses for applications requiring high quality tractography. Many of the methods developed to overcome the limitations of DTI, such as HARDI, require a larger number of diffusion weighted gradients and hence a longer acquisition time. However, in this study we found that POAS could in some degree compensate for the effects of a high angular resolution by improving the reliability and maintaining the tract volume and pathway. It can be used to reduce the number of applied diffusion gradients and acquisition time while achieving a similarly stable image quality, or to improve the quality of the image acquired with a feasible acquisition time. As reported, angular resolution plays a more important role in the improvement of the quality of tractography than spatial resolution when the acquisition time is limited in a clinical setting (*Zhan et al. 2013*). Therefore, with its effect on improving the stability of tractography in the CST while enhancing the SNR and not increasing the acquisition time at the same time, POAS should be a candidate in clinics and in the future the real application of POAS in pathological cases should be investigated. Nonetheless, some limitations associated with POAS also exist. After denoising with POAS, the FA value decreased significantly as well as the fiber density in the tractography of the CST. We made a simple schematic diagram to illustrate this situation (Fig.14). There was no loss in tract volume in CST-POAS when compared with CST-origin, but the fiber density of CST-POAS was less. Although the spatial occupation of the streamline, which also represents the fiber volume, plays a more important role in the guidance of neurosurgical operations to help avoid damaging of functional brain structures, the fiber density might be considered to reflect the dynamic changes in the microstructures in neurologic diseases. Therefore, in this situation other methods or more advanced approaches should be developed to help to make some improvements in fiber density detection.

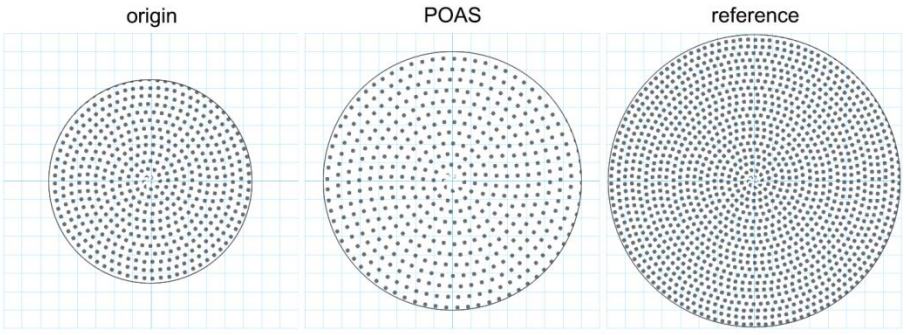

Fig.14: Illustration of tract volume and fiber density in the CST. The CST-POAS had a larger volume than CST-origin and CST-reference, but the fiber density in CST-POAS was also the smallest. The CST-reference presented the largest tract volume and fiber density.

4.3 General discussion of both parts

We discussed the two approaches separately, cardiac-gating and POAS, in optimizing the DWI, diffusion tensor metrics and tractography. These two approaches have different principles and contributions. We created a simple form to compare the similarities and differences between these two approaches (Table 5).

The DWI modification with cardiac-gating occurs during acquisition so it may prolong the acquisition time for individuals. While as a post-process technique, POAS improves the DWI after acquisition and the long processing time is irrelevant to the patients' condition. As for the improvement to DWI, both cardiac-gating and POAS are able to optimize image quality and decrease the signal variation. However, the effects are different. Cardiac-gating eliminates the artifacts produced by pulsatile motion, but the obvious background noise normally produced by echo planar imaging technique always remains. With POAS, after normal DWI acquisition, it is able to decrease the background noise and improve the SNR significantly. However, when pulsatile motion induces a prominent signal loss in a local region, POAS is unable to compensate for these changes. So these two approaches are based on different principles and modify DWI differently.

In the improvement of the diffusion tensor parameters, both cardiac-gating and POAS decreased the FA value, which was proven to correct the overestimation of FA in normal DWI acquisition. However, cardiac-gating did not affect the tract volume of the reconstructed CST,

while POAS was able to increase the tract volume of the CST. Therefore, modification of the entire brain with a significant increase of the SNR in POAS may make more improvement than cardiac-gating which makes local repair on brain, although cardiac-gating already focuses on mending the regions of the CST pathway. The POAS also decreases the tract variability while cardiac-gating does not have this effect.

Both of these two approaches were compared with the averaging method, which is easy to implement. Image averaging may denoise random artifacts and increase the SNR. Pulsatile motion artifacts also disappeared after averaging, in agreement with cardiac-gating. However, compared with averaging, POAS produced higher SNR, larger modification in diffusion metrics. On tractography, both POAS and averaging were able to increase the tract volume, but the shape of reconstructed CST in POAS was more like the reference approach which used more advanced algorithm. Although averaging could be an effective method to optimize the DWI and DTI analysis, it requires multiple DWI acquisitions and requires a longer time of acquisition, which may hinder its use in some patients who cannot bear extended usage of the MRI scanner. Both cardiac-gating and POAS have their cons and pros, and maybe more advanced optimized approaches should be investigated and applied.

Table 5: Comparison between the effect of cardiac-gating and POAS

Comparison (with original datasets)	**Cardiac-gating**	**POAS**
Time point of modification	during MRI acquisition	after MRI acquisition
DWI	image quality ↑ (no signal loss or signal attenuation) signal variation ↓	image quality ↑ (SNR↑↑) signal variation ↓
Diffusion tensor parameters of CST	FA↓, MD↑ L1—, L2↑, L3↑ V1↑ (from gradient direction to Z axis)	FA↓, MD↓
Tractography of CST	tract volume — tract variability —	tract volume ↑ tract variability↓ fiber density↓

Comparison with average	image quality —	image quality↑ (SNR↑) FA↓, MD↓ tract volume —

↑: increase compared to original datasets;

↓: decrease compared to original datesets;

—: no difference compared to original datasets

5. Summary

The corticospinal tract is important in the guidance of neurosurgery. Therefore precise tractography in the pre-operative plan is necessary. However, the inherent drawback of DWI in image acquisition makes it easy to be affected by bulk motion and pulsatile motion and also to produce image distortions because of EPI acquisitions. Therefore, optimized approaches aimed at reducing or eliminating these artifacts and improve image quality have been investigated.

Pulsatile motion occurs during the cardiac systolic period and has been reported to produce motion artifacts in the brain stem and basal ganglia, which might affect the corticospinal tract. Up to now, there is no consensus on the real effect of pulsatile motion on the diffusion properties, diffusion tensor parameters and fiber tractography, and the role of cardiac gating to overcome these effects is also not very clear. So in part 1 of the current study, we analyzed the influence of pulsatile motion and the contribution of cardiac-gating in the improvement of the quality of DWI, DTI and tractography. We found obvious signal attenuation in the brain stem and cerebellum. Pulsatile motion led to an over-estimation of FA and under-estimation of MD along the CST. Cardiac-gating could help to reduce the bias of the diffusion tensor parameters. Although pulsatile motion resulted in motion artifacts, bias of the diffusion tensor parameters and deviation of the principal eigenvector direction, it did not influence tract volume and location when a deterministic algorithm was applied for the reconstruction of the tract. Therefore, in this part we knew that cardiac-gating could help to avoid the motion artifacts and bias of the diffusion tensor parameters. But for the tractography of CST, the current image acquisition methods with high angular resolution or averaging seemed already able to overcome the effects of pulsatile motion, and cardiac-gating can’t make significant contribution.

In part 2 of this study, we focused on another approach for improving the DWI image quality, the denoising algorithm POAS (Position-orientation adaptive smoothing). The DWI suffers more easily from artifacts during acquisition and always has a low SNR, which might lead to

erroneous decisions in the determination of the diffusion metrics and fiber tractography in clinics. Although plenty of denoising methods have been proposed up to now, POAS came into consideration because POAS reduces image noise in the whole brain with edge-preserving properties and avoids blurring. In this study, we found that POAS reduced noise directly on DWIs and improved SNR dramatically, and consequently, POAS also reduced the bias and variation of the diffusion tensor quantities, such as FA. In tractography, after processing with POAS, a greater fiber volume of the CST was reconstructed compared to the original datasets. At the same time, reconstruction of the CST in POAS-processed datasets gained more stability and less variability which could compensate for the effect of a high angular resolution in some degree. In the future, the application of POAS in pathological cases should be conducted to verify its practical value in the clinics.

In neuroscience, the image quality of DWI and the precision of the diffusion tensor parameters are essential. Both of the above approaches could be applied to optimize the analysis. During neurosurgical operations, the accuracy of tract reconstruction, or space occupation, has more importance. So POAS could be considered to improve tractography while cardiac-gating did not have significant effects. More advanced approaches should be further investigated.

6. Zusammenfassung

Die maximal ausgedehnte Tumorvolumenreduktion bei gleichzeitigem Erhalt der neurologischen Funktion wird heute im mikrochirurgischen Behandlungskonzept von Hirntumoren als positiv prädiktiver Faktor für das Überleben der Patienten angesehen. Eine möglichst präzise und reliable Darstellung der Faserbahnsysteme ist dabei für die maximal sichere Tumorvolumenreduktion unerlässlich.

Die diffusionsgewichtete Bildgebung ist sensitiv gegenüber der Gefäßpulsation, die zu Bewegungsartefakten insbesondere im Bereich des Hirnstamms und der Basalganglien führt und somit vermeintlich Einfluss auf die Darstellung der Pyramidenbahnen nehmen kann. Bislang gibt es jedoch noch keinen Konsens über die Auswirkungen der Gefäßpulsation auf Diffusionstensorparameter und die Faserbahndarstellung an sich. Inwieweit eine pulsgetriggerte Datenakquisition dem entgegenwirkt ist ebenso noch weitgehend ungeklärt. In dieser Arbeit wurde daher der Einfluss der Gefäßpulsation und der pulsgetriggerten Datenakquisition in Bezug auf die Qualität der diffusionsgewichteten Bilddaten, der daraus resultierenden Diffusions-Tensor-Daten und Faserbahndarstellungen der Pyramidenbahnen analysiert. Dabei zeigten sich offensichtliche Signalabschwächungen im Bereich des Hirnstamms und des Kleinhirns und eine Überschätzung der fraktionellen Anisotropie und Unterschätzung der mittleren Diffusivität, wobei die pulsgetriggerte Datenakquisition den Einfluss auf die Diffusionstensorparameter reduzierte. Obwohl die Gefäßpulsation zu Bewegungsartefakten führte, die Diffusionstensorparameter beeinflusste und es zu einer Abweichung des ersten Eigenvektors kam, der für die Faserbahnrekonstruktion maßgeblich ist, zeigten sich auf Ebene der Faserbahndarstellung keine Unterschiede in Faserbahnvolumen und der räumlichen Lage der Pyramidenbahndarstellungen. Vermutlich trägt die heutige Datenakquisition mit hoher Winkelauflösung zur Stabilität der Faserbahndarstellung bei, so dass die pulsgetriggerte Datenakquisition zwar auf die Bewegungskorrektur in den diffusionsgewichteten Bilddaten selbst und die Diffusionstensorparameter einen Einfluss nimmt, jedoch für die Faserbahndarstellung keine deutliche Verbesserung zeigt.

Eine Schwäche der diffusionsgewichteten Bildgebung ist das niedrige Signal-zu-Rausch Verhältnis, die ebenso zu Veränderungen in der Modellierung des Diffusionsverhaltens und der Faserbahndarstellung führen kann. Um dies zu kompensieren und die Bildqualität der Ausgangsdaten zu erhöhen stehen verschiedenste Ansätze zur Verfügung. In der klinischen Bildgebung wird dabei häufig auf Messwiederholungen zurückgegriffen, was jedoch mit einem Vielfachen der Akquisitionszeit einhergeht. Eine alternative strukturerhaltende Glättung, das sogenannte position-orientation adaptive smoothing (POAS), kann bereits auf einem einzelnen Datensatz (ohne Messwiederholung) zur Reduktion des Bildrauschens angewendet werden. In dieser Arbeit wurden nun sowohl die Originaldaten als auch die gemittelten Daten aus fünf Messwiederholungen sowie die mittels POAS verarbeiteten Daten miteinander verglichen. Bereits in den diffusionsgewichteten Bilddaten zeigte sich für die Anwendung von POAS eine unmittelbare Reduzierung es Rauschens und eine Verbesserung des Signal-zu-Rausch Verhältnis, ebenso eine verringerte Variabilität der Diffusions-Tensor-Parameter. Für die Rekonstruktion der Pyramidenbahnen fand sich ein deutlich erhöhtes Faserbahnvolumen sowie eine höhere Stabilität der Rekonstruktionsergebnisse. Insbesondere aufgrund der Auswirkungen auf die Faserbahnrekonstruktion sollte in zukünftigen Studien auch die Anwendung bei Patienten mit Hirntumoren systematisch analysiert werden, um den klinischen Nutzen weiter zu verifizieren.

In den Neurowissenschaften werden Parameter verschiedensten Verarbeitungsschritte diffusionsgewichteter Bilddaten für Forschungszwecke herangezogen, Parameter der diffusionsgewichteten Bildgebung selbst, der Diffusion-Tensor-Modellierung sowie der Faserbahnrekonstruktionen und Faserbahneigenschaften. Die zugrundeliegende Bildqualität spielt dahingehend eine essentielle und womöglich entscheidende Rolle. Beide in dieser Arbeit untersuchten Ansätze können zur Optimierung der Bilddaten beitragen wobei insbesondere die strukturerhaltene Glättung mittels POAS Potential in Hinblick auf eine zuverlässigere und reliable Darstellung von Faserbahnen für die intraoperative Anwendung in der Neurochirurgie bietet.

7. References

Aja-Fernández S., Niethammer M., Kubicki M., Shenton M. E., Westin C.-F. (2008) Restoration of DWI data using a Rician LMMSE estimator. IEEE transactions on medical imaging 27:1389-1403

Anderson A. W. (2001) Theoretical analysis of the effects of noise on diffusion tensor imaging. Magnetic Resonance in Medicine: An Official Journal of the International Society for Magnetic Resonance in Medicine 46:1174-1188

Association W. M. (2001) World Medical Association Declaration of Helsinki. Ethical principles for medical research involving human subjects. Bulletin of the World Health Organization 79:373

Auriat A., Borich M., Snow N., Wadden K., Boyd L. (2015) Comparing a diffusion tensor and non-tensor approach to white matter fiber tractography in chronic stroke. Neuroimage: Clinical 7:771-781

Bammer R., Holdsworth S. J., Veldhuis W. B., Skare S. T. (2009) New methods in diffusion-weighted and diffusion tensor imaging. Magnetic resonance imaging clinics of North America 17:175-204

Basser P. J., Mattiello J., LeBihan D. (1994a) Estimation of the effective self-diffusion tensor from the NMR spin echo. Journal of Magnetic Resonance, Series B 103:247-254

Basser P. J., Mattiello J., LeBihan D. (1994b) MR diffusion tensor spectroscopy and imaging. Biophysical journal 66:259-267

Basser P. J., Pajevic S. (2000) Statistical artifacts in diffusion tensor MRI (DT-MRI) caused by background noise. Magnetic Resonance in Medicine: An Official Journal of the International Society for Magnetic Resonance in Medicine 44:41-50

Basser P. J., Pajevic S., Pierpaoli C., Duda J., Aldroubi A. (2000) In vivo fiber tractography using DT-MRI data. Magnetic resonance in medicine 44:625-632

Becker S., Tabelow K., Voss H. U., Anwander A., Heidemann R. M., Polzehl J. (2012) Position-orientation adaptive smoothing of diffusion weighted magnetic resonance data (POAS). Medical image analysis 16:1142-1155

Becker S., Tabelow K., Mohammadi S., Weiskopf N., Polzehl J. (2014) Adaptive smoothing of multi-shell diffusion weighted magnetic resonance data by msPOAS. NeuroImage 95:90-105

Bello L., Gambini A., Castellano A., Carrabba G., Acerbi F., Fava E., Giussani C., Cadioli M., Blasi V., Casarotti A. (2008) Motor and language DTI Fiber Tracking combined with intraoperative subcortical mapping for surgical removal of gliomas. Neuroimage 39:369-382

Calabrese E., Badea A., Coe C. L., Lubach G. R., Styner M. A., Johnson G. A. (2014) Investigating the tradeoffs between spatial resolution and diffusion sampling for brain mapping with diffusion tractography: Time well spent? Human brain mapping 35:5667-5685

Chang L. C., Jones D. K., Pierpaoli C. (2005) RESTORE: robust estimation of tensors by outlier rejection. Magnetic Resonance in Medicine: An Official Journal of the International Society for Magnetic Resonance in Medicine 53:1088-1095

Chang L. C., Walker L., Pierpaoli C. (2012) Informed RESTORE: a method for robust estimation of diffusion tensor from low redundancy datasets in the presence of physiological noise artifacts. Magnetic resonance in medicine 68:1654-1663

Chung S., Courcot B., Sdika M., Moffat K., Rae C., Henry R. G. (2010) Bootstrap quantification of cardiac pulsation artifact in DTI. Neuroimage 49:631-640

Einstein A. (1905) Investigations on the Theory of the Brownian Movement. Ann der Physik

Farrell J. A., Landman B. A., Jones C. K., Smith S. A., Prince J. L., van Zijl P. C., Mori S. (2007) Effects of SNR on the accuracy and reproducibility of DTI-derived fractional anisotropy, mean diffusivity, and principal eigenvector measurements at 1.5 T. Journal of magnetic resonance imaging: JMRI 26:756

Federau C., Hagmann P., Maeder P., Müller M., Meuli R., Stuber M., O'Brien K. (2013) Dependence of brain intravoxel incoherent motion perfusion parameters on the cardiac cycle. PloS one 8:e72856

Federau C., Meuli R., O'Brien K., Maeder P., Hagmann P. (2014) Perfusion measurement in brain gliomas with intravoxel incoherent motion MRI. American Journal of Neuroradiology 35:256-262

Gao W., Zhu H., Lin W. (2009) A unified optimization approach for diffusion tensor imaging technique. Neuroimage 44:729-741

Glozman T., Bruckert L., Pestilli F., Yecies D. W., Guibas L. J., Yeom K. W. (2018) Framework for shape analysis of white matter fiber bundles. NeuroImage 167:466-477

Greitz D., Wirestam R., Franck A., Nordell B., Thomsen C., Ståhlberg F. (1992) Pulsatile brain movement and associated hydrodynamics studied by magnetic resonance phase imaging. Neuroradiology 34:370-380

Guo A., Provenzale J., Cruz Jr L., Petrella J. (2001) Cerebral abscesses: investigation using apparent diffusion coefficient maps. Neuroradiology 43:370-374

Habib J., Hlinka J., Sotiropoulos S., Tench C., Auer D., Morgan P. Relevance of cardiac-gating in longitudinal diffusion weighted MRI studies. In: Proceedings of the 16th Annual Meeting of the ISMRM. Toronto, Ontario, Canada, 2008. p 3133

Habib J., Auer D., Morgan P. Do we need cardiac gating in brain-DTI at high (3T) and ultra-high (7T) field strengths. In: Proceedings of the 11th Annual Meeting of the ISMRM. Honolulu, Hawaii, USA, 2009. p 3523

Habib J., Auer D. P., Morgan P. S. (2010) A quantitative analysis of the benefits of cardiac gating in practical diffusion tensor imaging of the brain. Magnetic Resonance in Medicine: An Official Journal of the International Society for Magnetic Resonance in Medicine 63:1098-1103

Holmes C. J., Hoge R., Collins L., Woods R., Toga A. W., Evans A. C. (1998) Enhancement of MR images using registration for signal averaging. Journal of computer assisted tomography 22:324-333

Hua K., Zhang J., Wakana S., Jiang H., Li X., Reich D. S., Calabresi P. A., Pekar J. J., van Zijl P. C., Mori S. (2008) Tract probability maps in stereotaxic spaces: analyses of white matter anatomy and tract-specific quantification. Neuroimage 39:336-347

Jaccard P. (1901) Étude comparative de la distribution florale dans une portion des Alpes et des Jura. Bull Soc Vaudoise Sci Nat 37:547-579

Jones D., Pierpaoli C. Contribution of cardiac pulsation to variability of tractography results. In: Proc Intl Soc Magn Reson Med, 2005. p 222

Jones D. K. (2004) The effect of gradient sampling schemes on measures derived from diffusion tensor MRI: a Monte Carlo study. Magnetic Resonance in Medicine: An Official Journal of the International Society for Magnetic Resonance in Medicine 51:807-815

Jones D. K., Basser P. J. (2004) “Squashing peanuts and smashing pumpkins”: how noise distorts diffusion-weighted MR data. Magnetic Resonance in Medicine: An Official Journal of the International Society for Magnetic Resonance in Medicine 52:979-993

Jones D. K., Knösche T. R., Turner R. (2013) White matter integrity, fiber count, and other fallacies: the do's and don'ts of diffusion MRI. Neuroimage 73:239-254

Kan H., Miyati T., Kasai H., Arai N., Ohno N., Mase M., Shibamoto Y. (2014) Transfer characteristics of arterial pulsatile force in regional intracranial tissue using dynamic diffusion MRI: A phantom study. Magnetic resonance imaging 32:1284-1289

Kan H., Miyati T., Mase M., Osawa T., Ohno N., Kasai H., Arai N., Kawano M., Shibamoto Y. (2015) Dynamic state of water molecular displacement of the brain during the cardiac cycle in idiopathic normal pressure hydrocephalus. Computerized Medical Imaging and Graphics 40:88-93

Kang K. M., Choi S. H., Kim D. E., Yun T. J., Kim J.-h., Sohn C.-H., Park S.-W. (2017) Application of Cardiac Gating to Improve the Reproducibility of Intravoxel Incoherent Motion Measurements in the Head and Neck. Magnetic Resonance in Medical Sciences 16:190-202

Kim M., Ronen I., Ugurbil K., Kim D.-S. (2006) Spatial resolution dependence of DTI tractography in human occipito-callosal region. Neuroimage 32:1243-1249

Kim S., Pickup S., Poptani H. (2010) Effects of cardiac pulsation in diffusion tensor imaging of the rat brain. Journal of neuroscience methods 194:116-121

Kozák L. R., Dávid S., Rudas G., Vidnyánszky Z., Leemans A., Nagy Z. (2013) Investigating the need of triggering the acquisition for infant diffusion MRI: a quantitative study including bootstrap statistics. Neuroimage 69:198-205

Le Bihan D., Breton E., Lallemand D., Grenier P., Cabanis E., Laval-Jeantet M. (1986) MR imaging of intravoxel incoherent motions: application to diffusion and perfusion in neurologic disorders. Radiology 161:401-407

Le Bihan D., Breton E., Lallemand D., Aubin M., Vignaud J., Laval-Jeantet M. (1988) Separation of diffusion and perfusion in intravoxel incoherent motion MR imaging. Radiology 168:497-505

Le Bihan D., Poupon C., Amadon A., Lethimonnier F. (2006) Artifacts and pitfalls in diffusion MRI. Journal of Magnetic Resonance Imaging: An Official Journal of the International Society for Magnetic Resonance in Medicine 24:478-488

Lenglet C., Campbell J. S., Descoteaux M., Haro G., Savadjiev P., Wassermann D., Anwander A., Deriche R., Pike G. B., Sapiro G. (2009) Mathematical methods for diffusion MRI processing. Neuroimage 45:S111-S122

Lenz G. W., Haacke E. M., White R. D. (1989) Retrospective cardiac gating: a review of technical aspects and future directions. Magnetic resonance imaging 7:445-455

Madai V. I., Galinovic I., Grittner U., Zaro-Weber O., Schneider A., Martin S. Z., Samson-Himmelstjerna F. C. v., Stengl K. L., Mutke M. A., Moeller-Hartmann W. (2014) DWI intensity values predict FLAIR lesions in acute ischemic stroke. PLoS One 9:e92295

Manjón J. V., Coupé P., Concha L., Buades A., Collins D. L., Robles M. (2013) Diffusion weighted image denoising using overcomplete local PCA. PloS one 8:e73021

McNab J. A., Jbabdi S., Deoni S. C., Douaud G., Behrens T. E., Miller K. L. (2009) High resolution diffusion-weighted imaging in fixed human brain using diffusion-weighted steady state free precession. Neuroimage 46:775-785

Mohan J., Krishnaveni V., Guo Y. (2014) A survey on the magnetic resonance image denoising methods. Biomedical Signal Processing and Control 9:56-69

Mori S., Barker P. B. (1999) Diffusion magnetic resonance imaging: its principle and applications. The Anatomical Record: An Official Publication of the American Association of Anatomists 257:102-109

Mori S., Crain B. J., Chacko V. P., Van Zijl P. C. (1999) Three-dimensional tracking of axonal projections in the brain by magnetic resonance imaging. Annals of Neurology: Official Journal of the American Neurological Association and the Child Neurology Society 45:265-269

Murakami A., Morimoto M., Yamada K., Kizu O., Nishimura A., Nishimura T., Sugimoto T. (2008) Fiber-tracking techniques can predict the degree of neurologic impairment for periventricular leukomalacia. Pediatrics 122:500-506

Nagy Z., Hutton C., Alexander D., Deichmann R., Weiskopf N. Employing bootstrapping methods to examine the need for pulse triggering in diffusion-weighted imaging. In: Proceedings of the 16th Annual Meeting of ISMRM, Toronto, Canada ed, 2008. p 238

Nakamura T., Miyati T., Kasai H., Ohno N., Yamada M., Mase M., Hara M., Shibamoto Y., Suzuki Y., Ichikawa K. (2009) Bulk motion-independent analyses of water diffusion changes in the brain during the cardiac cycle. Radiological physics and technology 2:133-137

Nichols T. E., Holmes A. P. (2002) Nonparametric permutation tests for functional neuroimaging: a primer with examples. Human brain mapping 15:1-25

Nimsky C., Ganslandt O., Hastreiter P., Wang R., Benner T., Sorensen A. G., Fahlbusch R. (2005a) Intraoperative diffusion-tensor MR imaging: shifting of white matter tracts during neurosurgical procedures—initial experience. Radiology 234:218-225

Nimsky C., Ganslandt O., Hastreiter P., Wang R., Benner T., Sorensen A. G., Fahlbusch R. (2005b) Preoperative and intraoperative diffusion tensor imaging-based fiber tracking in glioma surgery. Neurosurgery 56:130-138

Nimsky C., Ganslandt O., Merhof D., Sorensen A. G., Fahlbusch R. (2006) Intraoperative visualization of the pyramidal tract by diffusion-tensor-imaging-based fiber tracking. Neuroimage 30:1219-1229

Nunes R. G., Jezzard P., Clare S. (2005) Investigations on the efficiency of cardiac-gated methods for the acquisition of diffusion-weighted images. Journal of Magnetic Resonance 177:102-110

O'Donnell L. J., Suter Y., Rigolo L., Kahali P., Zhang F., Norton I., Albi A., Olubiyi O., Meola A., Essayed W. I. (2017) Automated white matter fiber tract identification in patients with brain tumors. NeuroImage: Clinical 13:138-153

Parker G. J., Schnabel J. A., Symms M. R., Werring D. J., Barker G. J. (2000) Nonlinear smoothing for reduction of systematic and random errors in diffusion tensor imaging. Journal of Magnetic Resonance Imaging: An Official Journal of the International Society for Magnetic Resonance in Medicine 11:702-710

Penny W. D., Friston K. J., Ashburner J. T., Kiebel S. J., Nichols T. E. (2011) Statistical parametric mapping: the analysis of functional brain images. Elsevier,

Perona P., Malik J. (1990) Scale-space and edge detection using anisotropic diffusion. IEEE Transactions on pattern analysis and machine intelligence 12:629-639

Pierpaoli C., Basser P. J. (1996) Toward a quantitative assessment of diffusion anisotropy. Magnetic resonance in Medicine 36:893-906

Pierpaoli C., Marenco S., Rohde G., Jones D., Barnett A. Analyzing the contribution of cardiac pulsation to the variability of quantities derived from the diffusion tensor. In: Proceedings of the 11th Annual Meeting of ISMRM, Toronto, Canada, 2003. p 70

Polders D. L., Leemans A., Hendrikse J., Donahue M. J., Luijten P. R., Hoogduin J. M. (2011) Signal to noise ratio and uncertainty in diffusion tensor imaging at 1.5, 3.0, and 7.0 Tesla. Journal of Magnetic Resonance Imaging 33:1456-1463

Polzehl J., Spokoiny V. (2006) Propagation-separation approach for local likelihood estimation. Probability Theory and Related Fields 135:335-362

Radmanesh A., Greenberg J. K., Chatterjee A., Smyth M. D., Limbrick D. D., Sharma A. (2015) Tonsillar pulsatility before and after surgical decompression for children with Chiari malformation type 1: an application for true fast imaging with steady state precession. Neuroradiology 57:387-393

Rizzo G., Martinelli P., Manners D., Scaglione C., Tonon C., Cortelli P., Malucelli E., Capellari S., Testa C., Parchi P. (2008) Diffusion-weighted brain imaging study of patients with clinical diagnosis of corticobasal degeneration, progressive supranuclear palsy and Parkinson's disease. Brain 131:2690-2700

Roberts T. P., Liu F., Kassner A., Mori S., Guha A. (2005) Fiber density index correlates with reduced fractional anisotropy in white matter of patients with glioblastoma. American Journal of Neuroradiology 26:2183-2186

Robson M. D., Porter D. A. (2005) Reconstruction as a source of artifact in nongated single-shot diffusion-weighted EPI. Magnetic resonance imaging 23:899-905

Rueckert D., Sonoda L. I., Hayes C., Hill D. L., Leach M. O., Hawkes D. J. (1999) Nonrigid registration using free-form deformations: application to breast MR images. IEEE transactions on medical imaging 18:712-721

Scherer M., Jungk C., Götz M., Kickingereder P., Reuss D., Bendszus M., Maier-Hein K., Unterberg A. (2018) Early postoperative delineation of residual tumor after low-grade glioma resection by probabilistic quantification of diffusion-weighted imaging. Journal of Neurosurgery:1-9

Sener S., Van Hecke W., Feyen B. F., Van der Steen G., Pullens P., Van de Hauwe L., Menovsky T., Parizel P. M., Jorens P. G., Maas A. I. (2016) Diffusion tensor imaging: a possible biomarker in severe traumatic brain injury and aneurysmal subarachnoid hemorrhage? Neurosurgery 79:786-793

Skare S., Andersson J. L. (2001) On the effects of gating in diffusion imaging of the brain using single shot EPI. Magnetic resonance imaging 19:1125-1128

Smith S. M., Jenkinson M., Johansen-Berg H., Rueckert D., Nichols T. E., Mackay C. E., Watkins K. E., Ciccarelli O., Cader M. Z., Matthews P. M. (2006) Tract-based spatial statistics: voxelwise analysis of multi-subject diffusion data. Neuroimage 31:1487-1505

Smith S. M., Nichols T. E. (2009) Threshold-free cluster enhancement: addressing problems of smoothing, threshold dependence and localisation in cluster inference. Neuroimage 44:83-98

Stejskal E. O., Tanner J. E. (1965) Spin diffusion measurements: spin echoes in the presence of a time-dependent field gradient. The journal of chemical physics 42:288-292

Tabelow K., Mohammadi S., Weiskopf N., Polzehl J. (2015) POAS4SPM: a toolbox for SPM to denoise diffusion MRI data. Neuroinformatics 13:19-29

Tournier J.-D., Calamante F., Connelly A. (2007) Robust determination of the fibre orientation distribution in diffusion MRI: non-negativity constrained super-resolved spherical deconvolution. Neuroimage 35:1459-1472

Tournier J.-D., Yeh C.-H., Calamante F., Cho K.-H., Connelly A., Lin C.-P. (2008) Resolving crossing fibres using constrained spherical deconvolution: validation using diffusion-weighted imaging phantom data. Neuroimage 42:617-625

Tournier J. D., Mori S., Leemans A. (2011) Diffusion tensor imaging and beyond. Magnetic resonance in medicine 65:1532-1556

Tuch D. S. High angular resolution diffusion imaging of the human brain. In: Proceedings of the 7th Annual Meeting of ISMRM, Philadelphia, 1999, 1999.

Tuch D. S., Reese T. G., Wiegell M. R., Makris N., Belliveau J. W., Wedeen V. J. (2002) High angular resolution diffusion imaging reveals intravoxel white matter fiber heterogeneity. Magnetic Resonance in Medicine: An Official Journal of the International Society for Magnetic Resonance in Medicine 48:577-582

Tuch D. S. (2004) Q-ball imaging. Magnetic Resonance in Medicine: An Official Journal of the International Society for Magnetic Resonance in Medicine 52:1358-1372

Vos S. B., Aksoy M., Han Z., Holdsworth S. J., Maclaren J., Viergever M. A., Leemans A., Bammer R. (2016) Trade-off between angular and spatial resolutions in in vivo fiber tractography. NeuroImage 129:117-132

Walker L., Chang L., Kanterakis E., Bloy L., Simonyan K., Verma R., Pierpaoli C. (2009) Statistical assessment of the effects of physiological noise and artifacts in a population analysis of diffusion tensor MRI data. Proc Intl Soc Mag Reson Med Sci Meet Exhib 17:459

Walker L., Chang L.-C., Koay C. G., Sharma N., Cohen L., Verma R., Pierpaoli C. (2011) Effects of physiological noise in population analysis of diffusion tensor MRI data. NeuroImage 54:1168-1177

Wang J. Y., Abdi H., Bakhadirov K., Diaz-Arrastia R., Devous Sr M. D. (2012) A comprehensive reliability assessment of quantitative diffusion tensor tractography. Neuroimage 60:1127-1138

Warach S., Gaa J., Siewert B., Wielopolski P., Edelman R. R. (1995) Acute human stroke studied by whole brain echo planar diffusion-weighted magnetic resonance imaging. Annals of Neurology: Official Journal of the American Neurological Association and the Child Neurology Society 37:231-241

Weickert J. (1998) Anisotropic diffusion in image processing, vol 1. Teubner Stuttgart,

Westin C.-F., Maier S. E., Khidhir B., Everett P., Jolesz F. A., Kikinis R. Image processing for diffusion tensor magnetic resonance imaging. In: International Conference on Medical Image Computing and Computer-Assisted Intervention, 1999. Springer, pp 441-452

Wiest-Daessl é N., Prima S., Coup é P., Morrissey S. P., Barillot C. Rician noise removal by non-local means filtering for low signal-to-noise ratio MRI: applications to DT-MRI. In: International Conference on Medical Image Computing and Computer-assisted Intervention, 2008. Springer, pp 171-179

Winkler A. M., Ridgway G. R., Webster M. A., Smith S. M., Nichols T. E. (2014) Permutation inference for the general linear model. Neuroimage 92:381-397

Wirestam R., Bibic A., L ätt J., Brockstedt S., St åhlberg F. (2006) Denoising of complex MRI data by wavelet-domain filtering: Application to high-b-value diffusion-weighted imaging. Magnetic Resonance in Medicine: An Official Journal of the International Society for Magnetic Resonance in Medicine 56:1114-1120

Wu C.-C., Guo W.-Y., Chen M.-H., Ho D. M., Hung A. S., Chung H.-W. (2012) Direct measurement of the signal intensity of diffusion-weighted magnetic resonance imaging for preoperative grading and treatment guidance for brain gliomas. Journal of the Chinese Medical Association 75:581-588

Xie S., Zuo N., Shang L., Song M., Fan L., Jiang T. (2015) How does B-value affect HARDI reconstruction using clinical diffusion MRI data? PloS one 10:e0120773

Yamada K., Mori S., Nakamura H., Ito H., Kizu O., Shiga K., Yoshikawa K., Makino M., Yuen S., Kubota T. (2003) Fiber-tracking method reveals sensorimotor pathway involvement in stroke patients. Stroke 34:e159-e162

Yeatman J. D., Dougherty R. F., Myall N. J., Wandell B. A., Feldman H. M. (2012) Tract profiles of white matter properties: automating fiber-tract quantification. PloS one 7:e49790

Yoshiura T., Mihara F., Tanaka A., Ogomori K., Ohyagi Y., Taniwaki T., Yamada T., Yamasaki T., Ichimiya A., Kinukawa N. (2003) High b value diffusion-weighted imaging is more sensitive to white matter degeneration in Alzheimer's disease. Neuroimage 20:413-419

Zhan L., Leow A. D., Jahanshad N., Chiang M.-C., Barysheva M., Lee A. D., Toga A. W., McMahon K. L., De Zubicaray G. I., Wright M. J. (2010) How does angular resolution affect diffusion imaging measures? Neuroimage 49:1357-1371

Zhan L., Jahanshad N., Ennis D. B., Jin Y., Bernstein M. A., Borowski B. J., Jack Jr C. R., Toga A. W., Leow A. D., Thompson P. M. (2013) Angular versus spatial resolution trade-offs for diffusion imaging under time constraints. Human brain mapping 34:2688-2706

Zhang W., Olivi A., Hertig S. J., Van Zijl P., Mori S. (2008) Automated fiber tracking of human brain white matter using diffusion tensor imaging. Neuroimage 42:771-777

Curriculum Vitae

Personal information

Name: Jia Yang

Date of birth: 09.08.1991

Gender: Female

Place of birth: Henan, VR China

Nationality: China

Education

Dec 2016 – now Doctor's degree in medicine

Department of neurosurgery, Marburg Philipps University, Marburg, Germany

Sep 2009 – Jul 2016 Bachelor's and Master's degree in medicine

Seven-year program in medical school, Nankai University, Tianjin, China

Sep 2006 – Jul 2009 NO.16 high school in Zhengzhou

Zhengzhou, China

Sep 2003 – Jul 2006 NO.3 junior school in Xinye

Xinye of Henan, China

Sep 1998 – Jul 2003 The elementary school in Xinye

Xinye of Henan, China

Clinical training

May 2015 – Jul 2016 neurosurgery training

Department of neurosurgery, Chinese PLA general hospital, Beijing, China

Jun 2014 – May 2015 rotation in internal and surgical medicine

Chinese PLA general hospital, Beijing, China

Publication

Bopp MHA*, Yang J*, Nimsky C, Carl B. The effect of pulsatile motion and cardiac-gating on reconstruction and diffusion tensor properties of the corticospinal tract. *Sci Rep*. 2018;8(1):11204. Published 2018 Jul 25. doi:10.1038/s41598-018-29525-0

Conferences

Yang J.*, Bopp M. H. A*, Carl B., Nimsky C. (2018) Effect of pulsatile motion on brain diffusion tensor parameters. 69. Jahrestagung der Deutschen Gesellschaft für Neurochirurgie (DGNC). Münster, 03.-06.06.2018.

Yang J.*, Bopp M. H. A*, Carl B., Nimsky C. (2019) The influence of a denoising algorithm on diffusion tensor metrics in diffusion weighted imaging (DWI). 70. Jahrestagung der Deutschen Gesellschaft für Neurochirurgie (DGNC). Würzburg, 12.-15.05.2019.

Yang J.*, Bopp M. H. A*, Carl B., Nimsky C. (2019) The contribution of a denoising algorithm in diffusion weighted imaging (DWI): the effect on tractography of corticospinal tract. 70. Jahrestagung der Deutschen Gesellschaft für Neurochirurgie (DGNC). Würzburg, 12.-15.05.2019.

Yang J.*, Bopp M. H. A*, Carl B., Nimsky C. (2019) The reproducibility of fiber tractography of the corticospinal tract using manual and automatic tractography. 70. Jahrestagung der Deutschen Gesellschaft für Neurochirurgie (DGNC). Würzburg, 12.-15.05.2019

* Bopp MHA and Yang J contributed equally.

List of academic teachers

My academic teachers are in Marburg: Prof. Dr. Christopher Nimsky, and Dr. Miriam H.A. Bopp, and in China: Prof. Dr. Xiaolei Chen and Prof. Dr. Yongzhe Che.

Acknowledgement

First of all, I would like to thank Prof. Nimsky for giving me the opportunity to study here in Germany. His trust gives me the encouragement to continue the study all the time. I would also give my sincere thanks to Dr. Bopp, who helps a lot. Whenever I meet some problems in study that I really can't solve, she often could enlighten me and give me useful advice.

I also want to thank Alexandra Alina Kerl. She began her doctoral study in the same year with me. She has given me much nice information about the local culture and life and that is really helpful for me to adapt to the life here. The time we discussing studies together are worth remembering.

I would like to thank all the friends and families who have given me any support and comfort in study and life. As a person with clumsy speech, I don't often express my thanks orally but all gratitude is never forgotten. I would like to thank my friend Yining Zhao. That time we have travelled in Europe together is also a big treasure of my life.

I would like to thank the Chinese Scholarship Council. They afford my expense here so that I can study and enjoy life without any concern.

Although neuroimaging is my interest, starting as almost a fresh hand is never an easy thing. Whether I have tried everything is often a question that I ask to myself. I would thank myself for the patience and perseverance so that I can handle many skills today.

The more you know, the more you know you don't know, Aristotle said. Doctor's degree only marks the beginning of my research study.